Contribution „**Colloidal Particles at Liquid Interfaces**“
edited by B.P. Binks and T.S. Horozov, Cambridge University Press (2006)
pp. 445 – 499

Metal foams
towards high-temperature colloid chemistry

Norbert Babcsán and **John Banhart**
Hahn-Meitner-Institut Berlin, Glienicker Str. 100, D-14109 Berlin
and
Technical University Berlin, Institute of Materials Science and Technology,
Hardenbergstr. 36, D-10632 Berlin

1 Introduction

Liquid foams are collections of gas bubbles uniformly dispersed in fluids and separated from each other by self-standing thin films. If the distance between bubbles is comparable to the bubble size one prefers to speak of *bubble dispersions*. In foams, bubble arrangements are usually disordered and gas volume fractions are high. If a liquid foam is solidified a *solid foam* is obtained. Solid foams show many interesting properties which is the reason for their wide use, e.g. in civil engineering, chemistry or food industry [1].

Any liquid matter should be foamable and so liquid metal. The prospect of being able to make light durable metallic foams triggered research already more than half a

century ago. In 1948 Benjamin Sosnick [2] attempted to foam aluminium with mercury. He first melted a mix of Al and Hg in a closed chamber under high pressure. The pressure was released, leading to vaporisation of the mercury at the melting temperature of aluminium and to the formation of a foam. Less hazardous processes were developed in the mid 1950's when it was realised that liquid metals could be more easily foamed if they were pre-treated to modify their properties. This could be done by oxidising the melt or by adding solid particles. William Elliott [3] at Bjorksten Research Laboratories (BRL) developed an aluminium foaming process in the 1950's. BRL subsequently entered into an agreement with the LOR Corporation to develop commercial uses for foamed aluminium. A pilot plant was constructed at BRL to produce large wall panels. Other potential uses, such as crush bumpers for cars, were also investigated. In the late 1960's, the entire operation was sold to the Ethyl Corporation and the pilot plant was moved to Baton Rouge. BRL continued for several years to investigate methods for foaming other metals such as lead and zinc.

Two methods for foaming metals were used in those days, and they are still current today [4]. In the first of these, gas is injected continuously to create foam. The foam accumulates at the surface of the melt and the result somewhat looks like a glass of draught beer. In the second method, gas-releasing propellants are added to the melt, akin to the yeast of the baker (see **Figure 1**). Aluminium was found to be particularly amenable to foam production. The Ethyl Corporation produced material of remarkably high quality which was given to the Ford Motor Company for evaluation. Why was this initial development not successful? Certainly it was not the time for light-weight materials in the era of seemingly unlimited energy supply, and issues of safety and recycling were not so important as now. Whatever the reason, the excitement and the level of R&D activities both declined after 1975.

Figure 1. left: aluminium foam blown with air from a particle-stabilised melt and beer, right: zinc foam and bread roll, both foamed by internal gas creation (Photographs: HMI)

By the end of the 1980's there was a resurgence in metal foam research throughout the world. Japanese engineers at Shinko Wire Co. developed what is now known as the *Alporas* process [5]. Norsk Hydro in Norway [6] and Alcan Corp. in Canada [7] independently developed a foaming process for particle-stabilised melts. In 1990 an old powder-compact foaming route developed in the late 1950's by Benjamin Allen [8] was rediscovered and brought to a considerable level of sophistication at the

Fraunhofer Laboratory in Bremen, Germany [9]. These and other variants have been continually refined up to the present day [10,11].

Today a small number of companies produce aluminium foams. To our knowledge there are three in Germany, two in Austria, one each in Japan, Korea and Canada [12]. Here we do not count manufacture of cellular metals by sintering, electroplating or casting. The corresponding structures are frequently called *foams* but actually belong to a quite different class of materials. There are some applications for aluminium foams now including stiffening parts for cars, crash bumpers for light railways, a lifting arm for a lorry and stiff beams for working machines [13]. The market is still very small but slowly expanding.

The scientific challenges now are to improve foam properties and to make the production process more reliable. For this some knowledge of foam stability is indispensable. Surprisingly, research on the physics of metal foaming is quite restricted. Of about 300 journal papers listed on a dedicated web site [12] only about 20 are concerned with investigations of liquid metal foams, the remaining concentrating on processing, properties and applications of solid foams. Only very recently the issue of metal foam stabilisation was addressed and traced back to the presence of micro- or even nanometre-sized solid particles in the liquid metal [14].

The time has come to understand liquid metal foams as an independent field of research and to look at these systems under the viewpoint of colloid chemistry.

2 The making of metal foams

2.1 Processing routes

There are many ways to make metal foams and the various methods can be classified in different ways. For the purpose of this treatise the classification given in **Table 1** is particularly useful. We shall concentrate on aluminium alloys in the following although the phenomena which will be discussed occur for other metals too. As already mentioned in Sec. 1 we distinguish the way the gas comes into the melt, i.e. the gas source (1st column in the figure). Bubble creation can be *internal* or *external*. In the former case gas bubbles are created by gas evolution from within the melt. Nucleation of dissolved gas triggered by changes in pressure or temperature are a possible mechanism, the decomposition of a chemical blowing agent another. Often hydrides or carbonates are used as blowing agents in which case hydrogen or carbon dioxide evolve from the blowing agent. Alternatively, chemical reactions in the melt can create, e.g., water vapour which then drives foam expansion. In contrast, external bubble creation is caused by injecting gas into the melt continuously from outside, e.g. through a capillary or a porous frit. Clearly, the two methods imply different rheological phenomena during foaming as the bubbles are created at many locations in the melt in the former case while they have to travel a certain distance in the latter, usually from the injection point to the surface.

Table 1. Classification of metal foam making processes. For each of the eight possible categories either a company, trade or process name or a reference is given.

type of gas source	type of melt			
	pure melt	particles added	particles created in-situ	molten powder compact
internal	Pötschke [16] AMF [18] Gasar [19] / Lotus [20]	Formgrip [24] Foamcast [25]	LOR, Ethyl [26,27] Alporas [5] VFT [28] DCP [29,30]	Alulight/Foaminal [8,9,15] Thixofoam [31]
external	trial described in Ref 17	Alcan [7], Hydro [6] Metcomb [22]	trial by the authors	trial by the Authors

Another feature which can be used for classification is the type of melt which is foamed. In the simplest case we deal with a pure molten metal (2nd column). It is known from water that it is hard to make a foam from pure liquids and this is also true for metals. If bubbles are created in a pure melt they quickly rise to the surface and vanish there. Approaches to overcome this problem include creating bubbles in a melt by chemical reactions under weightlessness [16]. However, even in the absence of any buoyancy force one observes that bubbles tend to coalesce quickly in such systems and no foam with a significant and uniform porosity is obtained. Another approach involved bubbling argon gas through a highly pure magnesium melt while keeping the temperature near the melting point – and viscosity as high as possible – and solidifying while bubbling continued [17]. A certain level of porosity would be preserved but the resulting material could not really be called a foam. A related processing route has been investigated recently. In the so-called amorphous metal foaming (AMF) process, highly viscous bulk amorphous glass was foamed by internal gas formation and a quite high porosity level was obtained [18]. A further approach is the *Gasar* or *Lotus* process [19,20]. Gas is dissolved in a melt under high pressures and is then solidified directionally. One observes gas nucleation at the solidification front. Gas bubbles are pinned to the already existing pores so that they cannot float to the surface but form large and elongated pores. Again, temperature control prevents the bubbles from escaping but no real foam is obtained. Another strategy known from the literature is “foaming” a solid directly by creep expansion [21] which we shall not further consider here.

Scientists quickly began to realise that gas bubbles in pure melts are too volatile and too prone to coalescence to allow for making stable metallic foams. It is common knowledge in metal processing that porosity in castings or welding seems can be quite large and unwanted porosity is especially notorious when the metal to be cast or welded contains a high degree of non-metallic impurities. One therefore suspected that the presence of solid particles in the melt can help tackling problems of foam stability. Such solid particles can be brought into the melt either by simply admixing them to the melt (3rd column), by in-situ creation in the melt (4th column), or by making use of the oxidised surface layer of metal powers which are used during processing (5th column). We shall now describe some of the various possibilities not in a historical but more in a logical order.

If metal matrix composites (MMCs) containing a high volume fraction (10-20 %) of oxide or carbide particles are melted one obtains a suspension of these particles in the melt. Gas injection through a nozzle, frit, impeller etc. then leads to bubbles that rise

to the surface and form a stable layer of foam there. The bubbles are still buoyant but coalescence has been reduced to a minimum by the addition of particles. This foaming route was developed simultaneously by Alcan and Hydro Aluminium in the late 1980s who used aluminium alloys and silicon carbide particles. A technology called *Metcomb* [22] uses a similar approach and allows for a manufacture of very uniform pore morphologies as shown in **Figure 2a**.

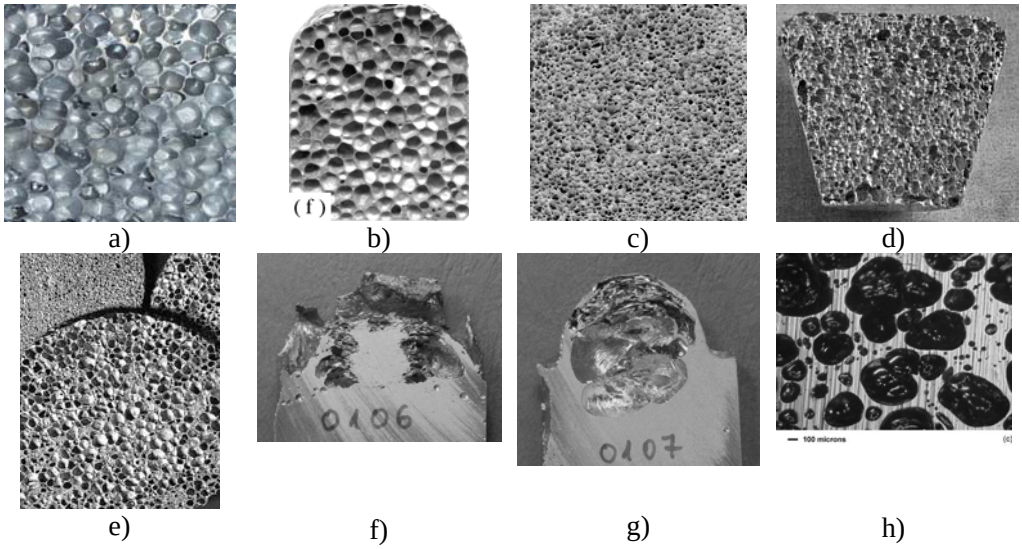

Figure 2. Macrostructures of various metal foams;
a) *Metcomb* Al-foam (courtesy D. Leitlmeier), b) Formgrip Al-foam [24], c) Alporas Al-foam [10], d) VFT Mg-foam [28], e) Alulight Al-foam [23], f) Alporas alloy foamed by gas injection, g) melted powder compact foamed by gas injection, h) Amorphous metal foam (Pd-based) [18].
Width of picture is a) 20 mm, b) 30 mm, c,d) 80 mm, e) 60 mm, f,g) 30 mm, h) 2 mm

The same MMC's can be used for foam making using an internal gas source instead of injecting gases. In the so-called *Formgrip* process [24] a blowing agent (titanium hydride, TiH_2) is added to a molten MMC. After sufficient stirring the melt is solidified. Owing to a prior pre-treatment of the hydride, gas evolution during stirring is not too pronounced and the solidified precursor contains less than 14% pores. The actual foam making step comprises re-melting of the precursor and holding at a baking temperature at which the blowing agent decomposes according to $TiH_2 \rightarrow Ti + H_2$. Unlike blowing gas through a nozzle gas bubbles are now created simultaneously in the entire volume by the decomposing hydride particles. The bubbles grow to a stable and uniform foam (see **Figure 2b**). An alternative technique mixes particle-free aluminium alloys and titanium hydride in a die-casting machine [25]. Due to rapid solidification there is no need for to use pre-treated TiH_2 in this *foamcast* method. To improve foamability of the precursor some alumina or oxidised aluminium powder is admixed to the blowing agent prior to injection.

Instead of preparing suspensions of particles in liquid metals one can condition melts in a different way to form stable foams. One idea was to create particles in the melt deliberately by in-situ reactions, e.g. oxidation. In the Japanese *Alporas* process calcium metal is added to an aluminium melt after which the melt is stirred in the presence of air for some minutes during which oxide particles are formed in-situ in

the melt [5]. After this, TiH_2 is added to the conditioned melt and dispersed by stirring. The hydride sets free hydrogen and turns the molten metal into a highly porous foam (see **Figure 2c**). Historically this was the way foams were successfully produced in the 1960s and 1970s, see, e.g., Refs [26,27]. At that time particles were created by bubbling, e.g., pure oxygen gas or water steam through the melt using rotating injectors or by admixing dry ice into molten Al 7-22 wt.% Mg alloy.

Quite recently a modification of this route was successfully demonstrated. Instead of creating particles in a well defined way, a contaminated magnesium melt was prepared by remelting casting overflows and machining chips which contained oxides, hydroxides, entrapped gas etc. TiH_2 as an internal gas source was substituted by pressure manipulation: The entire crucible containing the melt was placed in a chamber which then was evacuated. The pressure drop caused the gases dissolved or entrapped in the contaminated melt to expand and a quite regular foam was created in this so-called *vacuum foaming technique (VFT)* [28] (see **Figure 2d**).

Yet another way to create stabilizing particles was proposed recently [29]. A magnesium alloy containing about 10% alloying elements was processed in the semisolid state in a thixomolding machine. The melt was injected into a closed mould simultaneously with some MgH_2 serving as blowing agent. The mould was only partially filled to allow for foam evolution after injection. It was found that a metal foam evolved in the mould which could be taken out after rapid solidification. From the bubble size distribution as a function of local porosity the existence of a foam stabilisation mechanism was deduced. A similar approach was proposed for aluminium [30]. A normal die-casting machine is used for casting aluminium alloys. During melt injection MgH_2 powder is added. As for Mg the mixture of melt and blowing agent is allowed to evolve in the die. No addition of stabilising particles is mentioned for none of these *die-casting processing (DCP*) foaming routes. The particles – if existent – must then have been created in-situ during processing.

Another foaming method starts from metal powders. These are mixed with a blowing agent powder (usually TiH_2 for Al alloys) after which they are consolidated to a dense material by hot pressing or extrusion in the solid [15], or casting in the semi-solid state [31]. Remelting this material then triggers foam expansion as the blowing agent releases hydrogen. This processing route – called *Alulight* or *Foaminal* - is analogous to foaming by the *Formgrip* method already mentioned. Unlike the Formgrip method no particles have been added. Particles present in the melt are the former oxidised surfaces of the individual metal particles and they are obviously suffient for stanilisation. **Figure 2e** shows an Alulight sample made by this technique.

Table 1 shows two open positions which have not yet been discussed. The question is whether in-situ oxidised melts such as the ones used for making Alporas foams or remelted metal powder compacts without blowing agent can also be foamed by external bubble formation by gas injection through a nozzle. We carried out trials and received the “foams” shown in **Figure 2f and g**. Obviously foaming is more difficult here which we shall discuss later.

2.2 Stages of metal foam evolution

The term *foamability* quantifies how much and how good foam can be made from a liquid. The change of a foam from formation until collapse is called *foam evolution*. The evolution stages during foaming vary with the strategy chosen (e.g. external or internal gas injection). In most cases the temperature course during foaming includes

a heating stage, an isothermal holding stage and a cooling step. The principal stages are shown in **Figure 3**.

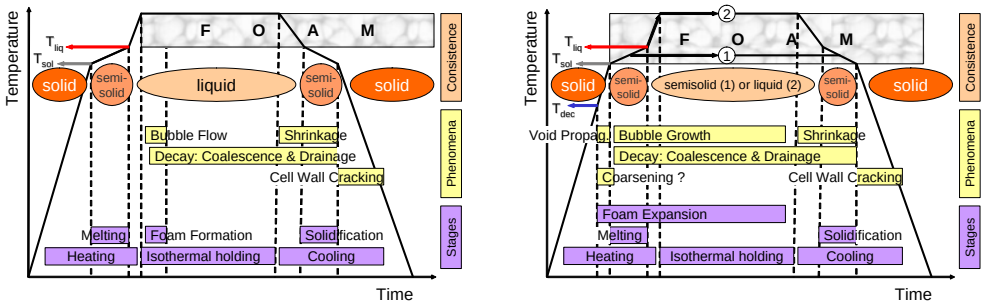

a) b)

Figure 3. Schematic representation of foam evolution as observed in a) foams made by external gas injection and, b) foams made by foaming precursors containing blowing agents, i.e. by internal gas generation.

Foaming with *external gas bubbling* (see **Figure 3a**) includes melting the alloy to be foamed, injecting gas – usually at a constant temperature – and then some further isothermal holding – either deliberately to study stability or to allow for processing the foam into shaped parts – , and then cooling to room temperature. During gas injection the bubbles rise from the injection point to the surface. After detachment from the injector the volume of the bubble changes in a well-defined way: heating of the gas contained in the bubble to the temperature of the liquid metal and the decreasing hydrostatic pressure during rise may lead to a certain expansion. We shall see later that during travelling the bubbles collect particles which adhere to the bubble surfaces. Provided that all parameters are right the bubbles are then stable and build up a foam layer. Decay phenomena can lead to changes in the foam layer during isothermal holding. Solidification can also influence foam structure.

Making foams utilizing a blowing agent – *i.e. internal gas bubbling* – can be more complicated. In **Figure 3b** the foaming stages are shown for the case that a precursor containing a blowing agent is melted. This applies to both the Formgrip-type and the Alulight-type foaming routes. In these foams the bubbles continuously grow during foaming due to the gas supplied by the blowing agent and due to thermal expansion. Expansion is governed by the continuous decomposition of the blowing agent (mostl a hydride or carbonate). Complicated relationships exist between the decomposition kinetics of the blowing agent and the melting of the alloys and kinetics depende on the particle size of the individual blowing agent particle. Therefore, bubbles are not expected to grow uniformly. A further complication are oxide layers which can be grown on the surface of blowing agent particles and which act as diffusion barriers to modify decomposition kinetics of the blowing agent [32].

If foaming is triggered by an external gas source the various stages of foaming can be well separated from each other. The actual foam formation takes only seconds after which the foam is usually held at a constant temperature. This facilitates studies of liquid foam and the interpretation of results. In contrast, during foaming of precursors containing a blowing agent foaming starts already during heating of the precursor and the gas supply depends in a complicated way on the decomposition kinetics of the blowing agent. Development of a fully expanded foam can requires several minutes.

The study of such foams is therefore more difficult since bubble nucleation and growth, drainage and coalescence overlap.

Other foaming processes such as the vacuum foaming technique or the Alporas process have foaming stages slightly different to the two considered. These processes are usually isothermal which facilitates their study slightly, but gas generation still follows a complicated law.

The range of phenomena in liquid foams is wide and they all influence one another. The main effects are drainage, coalescence, coarsening and flow. Their interdependence is indicated by arrows in **Figure 4**. Drainage, e.g., leads to coalescence since it gradually reduces the thickness of films and therefore increases the probability for an instability which eventually destroys the films. In metallic foams there is little coarsening due to the inability of gas to diffuse through the relatively thick films in the short times provided. One strategy in foam research is to eliminate some of these effects to be able to study the remaining ones. This is a strong motivation for using microgravity which avoids drainage. Low gravity experiments on metal foams were performed in TEXUS sounding rockets [33] or parabolic flights [34]. Flow of bubbles can be avoided by choosing stationary conditions in which foam expansion has come to an end. Under these circumstances coalescence can be studied without any disturbing interference.

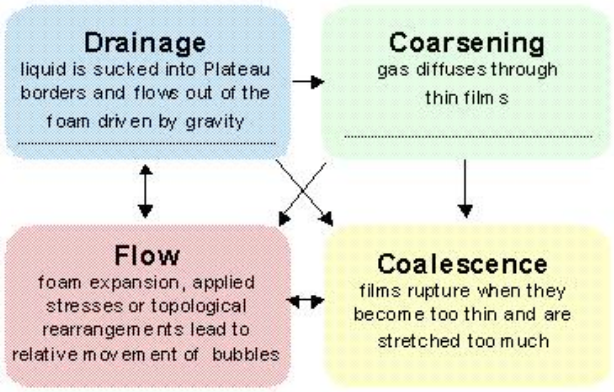

Figure 4. Phenomena which can occur during metal foam evolution [35].

3 Stabilisation of metal foams

3.1 Phenomenology of stabilisation

The term *foam stability* informs about the lifetime of a foam under given conditions and is related to the absence of cell wall rupture and to a limitation to drainage effects which eventually destroy foam structure. While phenomena related with aqueous foam stability are discussed in the literature in large monographs [36, 37, 38, 39, 40, 41, 42, 43, 44] work concerned with metal foams is still quite restricted [14, 34, 45, 46, 47, 48, 49, 50].

In Sec. 2.1. we saw that the manufacture of stable metal foams requires the presence of solid particles in the melt. This can also be shown by experiments in which a single metal film is produced by dipping a wire frame into a liquid and pulling it out. The attempt to produce a film from a particle-free aluminium melt with a wire frame fails

(**Figure 5a**). On pulling out the film ruptures immediately. The edge of the film remnant is only 2 μm thick. When the melt contains particles, however, stable liquid films can be pulled out by both vertically and horizontally arranged wire frames (**Figure 5b**). Thickness of these films is roughly the same as the average thickness of cell walls in foams made of the same material. This simple experiment is another convincing empirical evidence of the necessity of solid particles in stabilising thin liquid-metal films.

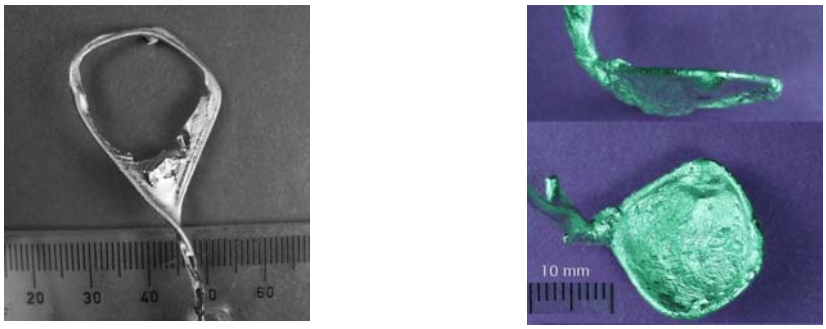

Figure 5. Pull-out tests with a wire frame; a) aluminium melt without particles; b) aluminium melt containing particles [46].

The large variety of metal foaming techniques demonstrates that the origin of these particles can be quite different ranging from added ceramic particles, oxides created in-situ in the melt, oxides originating from powder particles used in processing, to solid particles which are a natural component of any semi-solid melt. On the phenomenological level their necessity is evident although the way they act needs clarification.

While traditional aqueous foam can be considered colloidal systems because the diameter of the stabilising elements – e.g. the micelles –, is well below 1 μm, liquid-metal foams are stabilised by particles which cover a wide range of size. Mixing particles with liquid metals and achieving a uniform mixture is more difficult for small particles. Therefore, such systems only exist above 100 nm [51] particle size. In situ-oxidation techniques are not that restricted and allow for achieving smaller particles as e.g. for Alporas-type foams. Oxide remnants of powders used for processing are even smaller at least in one direction. The range of particles which has been used for foam stabilisation is listed in **Table 2**.

Table 2. Solid particles used for metal foam stabilisation.

particle class	colloid class	description	shape of particles	size range
added particles	liquid-metal *suspensions* → can sediment → no true colloids	MMC melt	smooth or angular polyhedron	0.1 – 50 μm
in-situ generated particles	liquid-metal *sols* → no sedimentation → true colloids	solid (endogenous) particles in melt	spherical	10 - 100 μm
		bi-films in melt	complex shaped	≈ 0.5 –10 μm
oxide remnants	liquid-metal *gels* → no sedimentation → true colloids	melted powder compacts	Irregular filaments	20 nm thick 50 μm wide

Figure 6 shows the size range which starts with 20 nm for the thickness of oxide filaments stabilising Alulight/Foaminal foams and ends with about 50 μm for the coarsest particles in Metcomb-type foams containing added SiC particles. In the former case we can therefore speak of high temperature *colloids*, while in the latter the term *suspension* seems more appropriate and we draw a somewhat artificial boundary at a value of 1 μm. It is interesting to note that the volume fraction of particles needed for foam stabilisation is related to their size. The larger the particles are the more one needs for effective stabilisation [46].

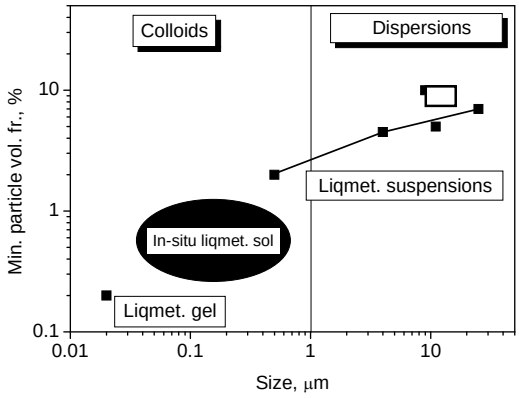

Figure 6. Size range of stabilising particles for metal foams of various types. For each size the volume fraction needed for stabilisation is shown [46].

3.2 Open questions and theoretical approaches

Often analogies between aqueous and liquid-metal foams are drawn. Pure single-component liquids cannot be foamed. Bubbles both in pure water and pure aluminium immediately rupture when they arrive at the surface. Adding surface active tensides, however, water becomes foamable and the same applies to metal foams when they are treated by one of the ways outlined in section 2.1. However, there are also obvious differences: Stable aqueous films can be made as thin as 6 nm (black film) [38], whereas metal foam films are rarely thinner than some tens of micrometers [31, 52]. The question is, why?

To prevent an aqueous film from thinning until rupture a local force is necessary which acts against local destabilisation caused by perturbations such as thermal fluctuations or surface waves. Tensides reduces surface tension but their main effect is to increase *surface elasticity*. In many types of foams the origin of stability is the Gibbs and Marangoni effect. The Gibbs effect occurs whenever a thin film is stretched and the film holds surfactant molecules in solution which lower surface tension. As stretching increases the surface area of the film the density of surfactant molecules per unit area of the film drops and surface tension increases. The Gibbs effect dictates that a stretched film will contract like an elastic skin. Hence, a force in the plane of the film occurs.

The Gibbs effect is quantified by a Gibbs elasticity E_G defined as:

$$E_G = -A\frac{d\sigma_{lg}}{dA} \quad (1)$$

where A is the surface area and σ_{lg} is the surface tension of liquid [53]. E_G ranges from 0.01 to 0.04 N/m [54] for water. Values for liquid alloys or liquid metal colloids are not yet known but should be determined.

There are also forces acting perpendicular to the films. The balance of such forces is quite complicated: beside attractive van der Waals forces there are repulsive forces – called *disjoining forces* – opposing film contraction. Electrical double layers on the film surfaces can generate such forces. The balance of these two forces describes foam stability in the so-called DLVO theory [55]. However, other forces such as hydration forces, steric forces, structural forces, peristaltic or hydrodynamic forces can also be important [56].

Aqueous foams can be also stabilised by *solid particles*: a) totally wettable particles present in Plateau borders slow down foam drainage; b) partially wettable particles form layers on the surface of the liquid films similar to surfactants [57]; c) colloidal particles form long-range ordered microstructures in the liquid films which are stabilised by a non-DLVO surface force called *structural force* [58]. The structural force appears during thinning of liquid films containing colloidal particles, e.g. surfactant micelles, macromolecules or solid particles. It origins from long-range interactions in concentrated colloidal dispersions. It is still a question how the particles – their action described by their concentration, their contact angle with the liquid-gas system, their size and shape – affect stability of liquid foams. However, the action of particles does not seem to be entirely clear.

Foam stability of a model system of water and 3.88 μm surface modified polystyrene particles was characterised by Wilson [59] as a function of the contact angle. The contact angle was set either by salt addition or by surfactants. Between 0-33° no foaming, between 33-67° slight foaming, between 67-85° good foaming and above 85° very good foaming was observed. In the presence of surfactants Johansson et al. examined the foam stabilising effect of micrometre-sized quartz particles. A stabilising effect was found in the range of 60-90° with an optimum at 75°. Below 44 μm particle size foam stability was enhanced with respect to larger particles [60]. Sun and Gao examined the effect of 1-75 μm PTFE, PE and PVC particles in surfactant free ethanol-water solution. The wetting angle of particles is tuned by setting the ethanol concentration. An optimum wetting angle range of 75° to 85° for obtaining stable foams was found. Smaller particles produced more stable foams [61]. Sethumadhavan et al. stabilised aqueous liquid films with 3-38.6 nm silica particles. It has to be noted that non-wetting particles are used even as antifoaming agents where the defoaming ability depends on both the contact angle - contact angles >90° leading to good defoaming - and the surface roughness of the particles [39]. An increase of particle concentration decreases the apparent surface tension of a water suspension [62].

In metal foams there are no electrostatic forces. The stabilisation mechanism must therefore be different. As metal foams contain solid particles it is near at hand to look for an analogy between the particle stabilisation mechanism of aqueous foams and metallic foams. While there is agreement that particles are needed for stabilisation, there is still some dispute about how particles act in metallic foams.

Table 3 gives an overview how foams based on different fluids are stabilised and what the most important properties of the fluid are.

Table 3. Summary of the properties of different foams.

	Water [38]	Polymer [83]	Glass [63]	Metal [31]
Surface tension of a one- component liquid, [mN/m]	78	4-30	500	1000
Viscosity of a one-component liquid, [mPa s]	1	100 - 2.5×10^{7}	100-1000	3
Cell wall thickness before rupture	6 nm (Newton black film)	400-850 nm	100 – 500 nm	20-30 μm
Surfactants	Surface-active molecules and/or particles	Silicone molecules or block copolymers	Glass forming and surface-active elements (P, Na, Si, B ...)	Particles

A *dynamic* picture of foam stability is e.g. proposed by Gergely et al. [49, 64] and states that the vertical motion of liquid can be damped by increasing the viscosity of the liquid by adding particles or by reducing the temperature to the range of the semi-solid state. Kumagai et al. suggested that solid particles in aqueous foams lead to flatter curvatures [65] around the Plateau borders which reduces suction of metal from the cell wall into the border. Viscosity was also held responsible for the observed stability of metal foams made by foaming powder compacts [66]. The films present in these foams contain up to 1 wt.% oxygen [67] which is thought to be present as thin oxide pockets around volumes of molten aluminium within the films. The idea is that although the liquid aluminium in the cell walls itself has a low viscosity the entire system behaves like an extremely viscous fluid because the molten aluminium is contained in the oxide pockets by capillary forces or by the mechanical barrier effect of oxides. Viscosity could even approach infinity if the oxides immobilised the metallic component in this way.

Körner et al. used a cellular automata model to show the effect of bulk viscosity and surface tension on foam evolution [68]. They found that neither increased viscosity nor decreased surface tension result in a stable foam. However, introduction of a disjoining force stabilises the system. The dynamic model was criticised by Körner [50] who pointed out that it could not explain the observed long-term stability of some foams and took this as a proof that a different explanation must apply.

Some modelling of metal foam stability started based on the concept of a metal foam containing isolated added particles. Jin's stability map was interpreted by Kaptay [69] on the basis of theoretical considerations. He pointed out that the wetting angle between particles and liquid has to be in a certain range for particles to be able to stabilise the gas/liquid-bubble interface. Using a *static* model of a 3D network of solid spherical particles he attempted to explain the force transfer between two interfaces of a foam and in this way stability via a disjoining pressure [70]. Various configurations of particles were considered in these models, of which three are shown in **Figure 7**. The basic idea is that a partially wetted particle is pinned to a surface since it has its lowest energy when immersed into the liquid at a given depth. A single layer of loosely packed particles (LP1), also discussed by Ip et al. [48], stabilises a film if the contact angle is below 90°. The two surfaces of the liquid are then pinned symmetrically to the particles. Two layers of particles (LP2) do an even better job. Whenever the contact angle is below 145° they keep the two surfaces well separated.

The attractive forces are compensated by the stiffness of the particles which are in touch. A third version of the model was proposed since the experimental evidence in many foams showed that the two layers do not touch in reality. In the LP2+C model the two surface layers are separated by mechanical bridges which are additional clusters (+C) of particles keeping the 2 layers apart.

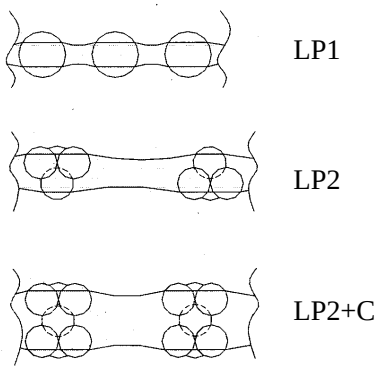

Figure 7. Possible particle configurations which could create a disjoining pressure: loosely packed single layer (LP1), loosely packed double layer LP2, loosely packed double plus layer (LP2+C) [70].

The distribution of particles and the forces acting between them are well known in aqueous suspensions. Their transparency and low melting point facilitate investigations. In high temperature systems such as metallic dispersions until now only post-solidification metallographic methods were available. In such studies one has to take into account that solidification might change the distribution, e.g. by the pushing effect or particle engulfment of a solidification front. It is hoped that new methods based, e.g., on synchrotron radiation and microfocus X-ray experiments could help establishing a new discipline called *high temperature colloid chemistry* which would then help to understand the stability of liquid-metal foams and *liquid-metal colloids (LMC)* in further detail.

In the next sections, we shall first summarise the physical properties of some ordinary melts and colloidal melts, and then collect and systematise experimental evidences of the action of colloidal particles in liquid metal foams.

4 Characterisation of liquids used for making metal foams

4.1 Surface properties

Various authors have published surface tension data of liquid aluminium and its alloys. The surface tension of metals is in general one order of magnitude larger that of water. A good overview can be found in Ref. 71. Most data were determined by the sessile drop or the maximum bubble pressure method [72,73,74]. In both cases results depend on the oxide layers which are hard to avoid on aluminium melt surfaces. At the melting point typical surface tensions of low-oxide and oxidised Al melts are 1.184 and 0.865 N/m, respectively [75].

The surface tension of oxidised Al is only weakly temperature dependent and changes from the melting point to 750°C only by -3% [73]. The main alloying elements of Al do not influence significantly surface tension. An addition of 1 wt.% Mg, e.g., reduces

surface tension by only 2.5 % [76]. Therefore, compared to the weak effect of metallic alloying elements oxidation has a strong effect by reducing surface tension by 27 %.

Kaptay analysed surface tension data of liquid Al_2O_3 and extrapolated this data to low temperatures. It was found that the surface tension of oxidised molten aluminium agreed with the extrapolated data of Al_2O_3 which indicates that oxygen covering the surface of molten aluminium resembles a supercooled state of Al_2O_3 [71].

The kinetics of oxidation depends on the oxygen partial pressure. Ricci et al. [77] estimated the time required to form an adsorbed oxygen monolayer on various metallic melts exposed to atmospheres containing different oxygen contents. An oxygen monolayer on molten tin, e.g., exposed to an atmosphere containing 1000 ppm, 1% and 10% of oxygen, forms in 44, 4.4 0.4 ms, respectively. Measurements of the surface tension of molten Sn/Pb solder as recently published by Howell et al. [78] using oscillating jets show the importance of progressing oxidation of melt surfaces.

Heterogeneous systems can be characterised by an apparent surface tension. Melt suitable for foaming – i.e. a suspension of ceramic particles in a liquid aluminium alloy – was investigated using a high-temperature maximum bubble pressure tensiometer. In this case Al containing a certain amount of alumina particles of 11 µm diameter was studied. It was found that increasing the Al_2O_3 particle content reduces surface tension which is an analogous effect to the oxidation effect mentioned above (see **Figure 8**).

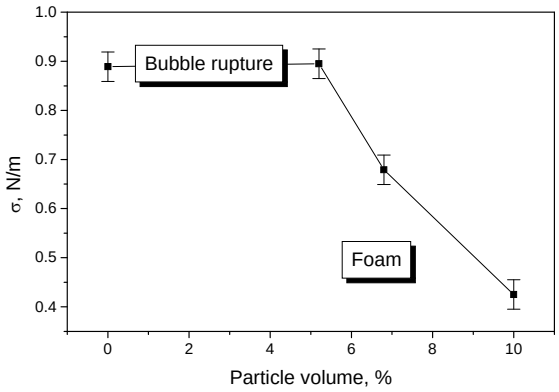

Figure 8. Apparent surface tension of Al melt (composition Si:0.4-0.8, Fe:0.7, Cu:0.3, Mn:0.004, Mg:0.74 in wt.%) as a function of Al_2O_3 particle content at 700°C [45].

Kommentar [JB1]: (surft_mmc)

4.2 Viscosity

Bulk viscosity of homogeneous liquid metals is comparable to that of water. According to the formula given by Andrade it increases with the atomic volume (V_m) and decreases with the atomic weight (M) and the melting point (T_m):

$$\eta = 1.8\times10^{-4} V_m^{3/2} \left(MT_m\right)^{1/2} \quad \text{[in mPa s]} \qquad (2)$$

Heterogeneous liquids can be described by an apparent or effective viscosity in many cases. One example are semisolid alloys. The presence of solidified primary α-

particles in the melt is known to increase viscosity [79]. For high solid fractions in the range of 50% such systems can exhibit a non-Newtonian flow behaviour with a shear rate dependent viscosity which has a practical relevance for thixo-casting or rheocasting.

Melts containing solid ceramic particles also show an increased bulk viscosity. This was measured for lead [80]. Melts produced by re-melting compacted lead powders containing oxidised surfaces have a viscosity which is more than twice as high as low-oxide lead melt (**Figure 9**).

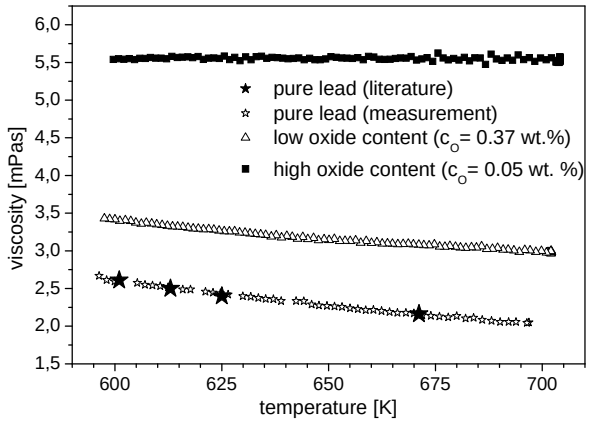

Figure 9. Bulk viscosity as measured by a rotational viscosimeter for pure Pb and two different Pb foam precursors [80].

Kommentar [JB2]: (wuebben viscPb)

The viscosity of the melts used for making Alporas foams – obtained by adding Ca to Al and allowing for some oxidation during stirring – can reach 10 times the value of the oxide free alloy depending on stirring time [81].

Table 4. Viscosities of various liquids.

(T_m= melting point, T_l= liquidus temperature, T_g = glass forming temperature)

Liquid metals	η [mPa s]	Ref.	Non-met. liquids	η [mPa s]	Ref.
pure Al at T_m	2 ± 0.8	[82]	Pure water at 20°C	1.025	[38]
pure Pb at T_m	2.61	[82]	Polymer melts	100-1013	[83]
pure Fe at T_m	6.92	[82]	Slag melt at 1500°C	200-300	[84]
melt of Pb powder, 0.37 wt.%, (0.05 wt.%) at T_m	5.5 (3.2)	[80]	Glycerine at 20°C	1508	[85]
Alporas melt at 720°C	1.5-14	[81]	Glass melt T= T_l	10000	[85]
AlSi6.5/SiC/10p at 700°C	30	[86]	Glass melt T> $T_{softening}$	5×10^9	[85]
AlSi6.5/SiC/20p at 700°C	50	[86]	Glass melt T> T_g	5×10^{16}	[85]
AlSi6.5/SiC/30p at 700°C	300	[86]			
Bulk met glass = T_l	1000	[18]			

MMC designations: alloy/particle/vol.%

Certain alloys can be transferred into a glassy state by continuous cooling from the liquid state. In some alloys this transition is obtained at very low cooling rates, e.g. less than 1 K/s. The viscosity of such alloys can reach very high values which has encouraged researchers to create foams from them [18]. Some typical viscosities of metallic and non-metallic liquids are listed in **Table 4**.

Viscosities of heterogeneous systems measured in a viscosimeter express an averaged behaviour of the liquid. In foams the composition of the liquid varies with higher particle concentrations near the surface of a film. Therefore, a gradient in viscosity can be expected with a surface viscosity above the average. The situation is even more complex in the compacted and re-melted powders which are used in the Alulight/Foaminal process. Here the meaning of the term viscosity is unclear. Films in the foams contain a network of oxide filaments which were created during powder atomisation. These filaments retain the liquid metal and lead to a very viscous appearance of the material which could possibly approach infinity if liquid flow is blocked completely. Upon stirring or shearing, however, the oxides agglomerate which changes conditions irreversibly [50]. Therefore, viscosity depends on history in this case and one should be very careful in using the term.

4.3 Reactions between particles and melt

Aluminium metal matrix composites (MMC) are the raw material of Cymat and Metcomb foams. Aluminium has a very high chemical reactivity in the liquid state. Al melt do not only react with most metals but also with some ceramics. Only if MMCs are made by a solid-state process interfacial reactions are not significant. If, however, liquid phase infiltration of ceramics or admixture of ceramic particles to a melt are applied to produce MMC [87] reactions are inevitable. The reaction temperatures and times during MMC production and aluminium composite melt foaming are similar which allows us to use the experience in MMC production for assessing the conditions during foaming.

Table 5. Chemical reactions of particles with Al melt below 1000°C.

Ceramics	Reaction with pure Al	Reaction products ,remarks	References
AlB_2	No	-	[88]
TiB_2	No	-	[88]
Carbon	depends on surface structure	(Al_4C_3)	[95, 96]
Al_4C_3	No	Al_4C_3 reacts with water forming CH_4	[95, 96]
B_4C	Yes	Al_3BC, AlB_2	[96]
SiC	Yes	Al_4C_3	[95, 96]
TiC	Yes	Al_4C_3, Al_3Ti	[96]
AlN	No	-	[89]
BN	Yes	AlN	[89]
Si_3N_4	Yes	AlN	[90]
Al_2O_3	No	-	[95, 96]
CaO	No	($CaAl_2O_4$ in the presence of O_2)	[91,92]
MgO	Yes	$MgAl_2O_4$	[93]
SiO_2	Yes	Al_2O_3, Al_2SiO_5, $Al_6Si_2O_{13}$	[95, 96]
TiO_2	Yes	Al_2O_3, AlTi, Al_3Ti, TiO	[94]

The reaction products often modify the surface of the particles in the melt resulting in a kind of coating. These coatings not only impair mechanical properties but also could influence foamability of such melts. Some common reaction data are summarised in **Table 5**. Among the materials listed the SiC and Al_2O_3 systems are most frequently used in practice. Some reactions can be both eliminated and promoted by alloying [95, 96].

SiC reacts with liquid Al [97]. The associated formation of aluminium carbide is detrimental to composite properties because of its brittleness and reactivity with water. It is also undesirable in the melt stirring process because it increases melt viscosity. Aluminium carbide formation can be prevented by adjustment of the matrix composition, by coating SiC particles with a physical barrier (Al_2O_3, TiO_2, TiB_2, SiO_2, TiC, TiN...), or by applying a sacrificial layer (Ni, Cu...) [96]. To prevent the formation of Al_4C_3 pure Al has to be alloyed with Si. The minimum Si content required for suppressing carbide formation was found to be 8.5 wt.% at 610°C and 13 wt.% at 825°C with a linear interpolation rule in between [98]. The presence of as little as 1 wt.% Mg in pure Al leads to the formation of Mg_2Si and facilitates the formation of aluminium carbide [99]. Contradictory to this in AlSi9Mg/SiC/10-20p the maximum overheating temperature was found to be 750°C which is 60°C higher than in the same alloy without Mg [98]. In the Al-SiC system above 1400°C Viala et al. found other complex carbides as Al_4SiC_4 and Al_8SiC_7 [100]. If SiC is oxidised the resulting SiO_2 surface layer can react with the liquid Al forming Al_2O_3, Al_2SiO_5 or $Al_6Si_2O_{13}$ (mullite). In the presence of Mg the reaction product is Al_2MgO_4 [101].

Al_2O_3 is stable in liquid aluminium but reacts in the presence of magnesium either to Al_2MgO_4 (spinel) for 1 wt.% < c_{Mg} < 4 wt.% or to MgO for c_{Mg}>4 wt.% [102]. The thin passivation layer of MgO prohibits further reactions. Detrimental spinel formation is continuous and can be limited by either, a) using a mixed oxide such as $Al_6Si_2O_{13}$ (mullite), b) forming a MgO barrier layer exploiting the reaction itself, c) using an aluminium matrix with a low magnesium content (c_{Mg}<1wt.%), or d) further alloying the Al matrix with an element like Sr which selectively segregates at the interface and inhibits spinel growth [103]. Al_2MgO_4 is observed for c_{Mg}>0.5 wt.% using infiltration casting but no reaction with squeeze casting. Schuster et al. reported interface spinel formation of AA6061/Al_2O_3/10-20p as well [104].

The thermodynamic stability range of reactions of liquid Al and ceramics as a function of alloying elements have been calculated and summarised in the literature (**Table 6**).

Table 6. Calculated thermodynamic stability range of reactions between liquid Al and ceramics.

Ceramic	Reaction products	Reaction stability range	Remarks
SiC	Al_4C_3	Below 7 at.% Si content at the melting point [105]	Increasing temperature and adding extra Mg the reaction stability range predicted by the model increases, good fit with experiments
Al_2O_3	$MgAl_2O_4$	0.02 wt.% < c_{Mg} < 1 wt.% at 700°C [106]	Calculation not explained in detail, the author's experimental findings agree with his calculation

4.4 Wetting of particles by melt

Wetting properties can be estimated by measuring the contact angle θ in sessile drop experiments with accuracies around 1° to 5°. θ can be calculated using the *Young equation*:

$$\sigma_{cl} = \sigma_{cg} - \sigma_{\mathrm{lg}} \cos\theta \qquad ()$$

where σ_{cg} is the ceramic particle/gas interface energy, σ_{cl} is the ceramic particle/liquid aluminium interface energy and σ_{lg} is the surface tension of the liquid. The *Young-Dupre equation* can also be applied

$$W = \sigma_{\mathrm{lg}}(1 + \cos\theta) \qquad ()$$

where *W* is the adhesion energy. The ceramic particle is perfectly wetted by the liquid at $\theta = 0°$ or $W \geq 2\sigma_{\mathrm{lg}}$. At $\theta < 90°$ the system is called *wetting*, while at $\theta > 90°$ it is *non-wetting*. The contact angle depends on time, temperature, composition, heat treatment of ceramics (impurity or absorbed gas removal), surface roughness [107] and atmospheric conditions during the experiment. For Al the oxide layers inevitably influence the measurements. Some examples for the contact angle of pure Al melt – particle – gas system (at 1100°C, no oxide layer on liquid Al, purified Ar atmosphere at 10^{-8} bar residual pressure, contacting time is not mentioned) are summarised in **Table 7** presenting exclusively wetting conditions [75].

Table 7. Contact angle of pure Al melt – particle – gas interface [75].

	TiB_2	WC	TiC	BN	SiO_2	SiC	graphite	Al_2O_3	TiN
θ, °	0	5	10	15	23	27	52	63	86

Among all metal/ceramic combinations, *Al-SiC* has been one of the most widely studied systems. The contact angle between aluminium and SiC can be modified by adding Si, Mg or Cu. The achievable changes can be as high as 40° for some compositions and temperatures. Si in liquid Al protects the SiC particles against interfacial reactions [108]. The change of the contact angle with time was measured in the system AlSi18/SiC at 800°C unter high vacuum 4×10^{-5} Pa [109]. The initial value was found to be 120°. SiC was so well protected against any reaction with Al by the high Si content of the melt that even after three hours the measured contact angle of 60° was twice as large then that of non alloyed Al melt (27°) [109]. The enhancement of wetting in the absence of Si is still not clear. Formation of Al_4C_3 is a possible explanation but the contact angle of 55° is even higher than the contact angle in SiC–Al melt (27°) [110].

Laurent et al. measured the dependence of the contact angle of the pure *Al - Al_2O_3* couple on oxygen partial pressure. Close to the melting point of Al the contact angle was 160° at 10^{-3} Pa but 100° at 10^{-5} Pa. Due to oxide layer evaporation at 900°C the pressure dependence of contact angle disappeared and decreased down to 90° [109]. Alloying with Li and Ca improved wetting due to the formation of complex Li or Ca aluminum oxides on the surface of the alumina particles and decreased surface tension (see Ref. [111], p. 51). The initial, i.e. shortly after the first contact, and time

dependent contact angle of (0001)-oriented α-Al_2O_3 single crystals under less than 5×10^{-4} Pa oxygen partial pressure were recently investigated. The contact angle was found to have a tendency to decrease with increasing temperature. Between 700 and 800 °C surplus *oxidation* was found without any essential change of contact angle. Heated above 800°C the pattern of oxygen on the (0001) plane varies from (1×1) to an oxygen deficient ($\sqrt{31}\times\sqrt{31}$ R±9°) Wood index structure while the contact angle decreases. Because of the reaction between Al melt and Al_2O_3 a strong decrease of wetting angle is observed above 1100°C. It was also found that while the contact angle of (0001) plane changes with time (at low temperature increasing-, at high temperature decreasing tendency) other crystallographic planes are not sensitive for the time. It can be summarised that 75° (30 min, 1500°C) seems to be the minimum and 130° for the maximum values of the contact angles (30 min, 700°C) [112].

5 Investigation of foaming process

Phenomena related to metal foam evolution and stability have been studied ex-situ after solidification or in-situ while the foam in still in its liquid state. Both methods are complementary. *Ex-situ* methods allow us to apply a larger variety of analytical tools but the evolution of foams has to be investigated by considering different samples representing the stages of foaming. In contrast, *in-situ* methods allow us to follow the evolution directly but are only available for a restricted set of analytical tools.

5.1 Ex-situ analysis of metallic foams after solidification

Ex-situ analysis of metal foams is an important tool for studying the microstructure and architecture of metal foams. By freezing the foam one hopes to preserve its morphological features and the arrangement of solid particles in the cell walls at least to a certain extent. One has to be aware of effects during solidification such as interactions of the solidification front with particles and pressure changes which might lead to a difference between the real situation in the foam and the picture obtained by analysing solid foams.

We shall now first analyse the microstructure of foams made by one of the processes listed in **Table 1**. We search for the particles responsible for stabilisation and for oxide films formed during foaming. Then the structure of cell walls will be analysed to reveal the influence of the stabilisation mode on thickness and shape of films.

5.1.1 Microstructure of foams and importance of particles

5.1.1.1 Added particles and external gas blowing (Metcomb-type foams)

In this type of metal foams it is most obvious that particles are responsible for liquid-metal foam stability. A first schematic stability map giving limits for particle content and particle size required for metal foam creation was published by Jin [7]. Ip et al. later found that particle attachment to the gas-liquid interface is necessary for the extended stability of the aluminium foam [48]. This occurs when after external gas injection bubbles travel through the liquid and interact with the dispersed particles, an effect analogous to flotation. Leitlmeier et al. [22] measured the volume fraction of particles in aluminium-based foams as a function of the travelling distance of bubbles in the melt - given by the distance from the injector to the metal surface - and found the stability criterion shown in **Figure 10**. Accordingly, below a critical travelling distance no stable foam could be produced since the bubbles did not collect enough

particles. The particle concentration in the cell walls increases up to a saturation value [22] because of the long travelling path of the rising bubbles in the MMC melt. After only some mm of rising in the MMC melt the SiC particles collected were only sufficient to cover the surfaces of the bubbles (**Figure 11a**). A longer travelling distance then yields a configuration with surface coverage plus some particle inside the cell wall (**Figure 11b**).

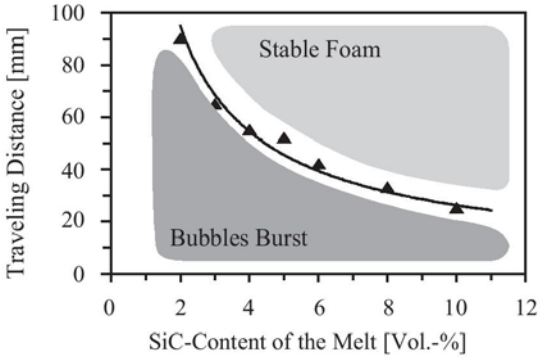

Figure 10. Effect of particle concentration and length of travelling path of bubbles through melt on foam stability [22].

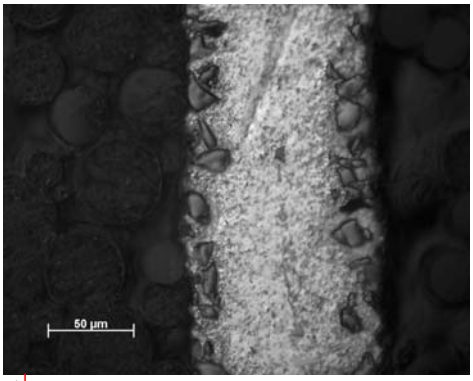

a)

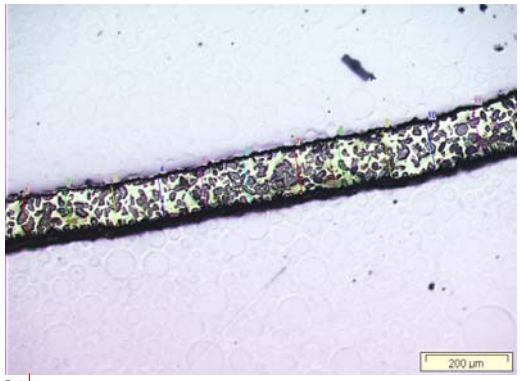

b)

Figure 11. Cell wall cross section of aluminium foam stabilised with SiC particles. The bubble rising height in the melt was a) 4 cm, b) 15 cm (Photos: HMI).

Kommentar [JB3]: (0022cw06).

Kommentar [JB4]: MN_A_22__07.

Interestingly, a meniscus of the melt around the particles located on the cell wall surface is not observed (**Figure 12**).

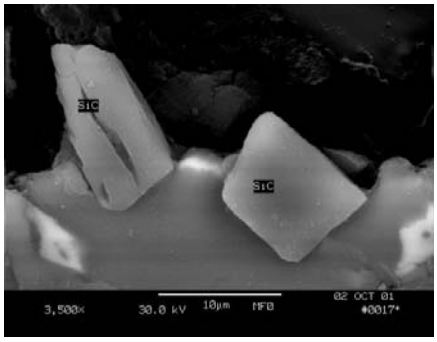

Figure 12. SiC particles at the surface of a Metcomb foam, cross section, SEM image (HMI).

Stable foams were successfully produced from aluminium alloy melts containing SiC and Al_2O_3 particles (MMC melts) [22]. It is interesting to note that Al_2O_3 particles were coated with nanometre-sized spinel (Al_2MgO_4) crystals in some successful foaming experiments in which the melt contained magnesium [47]. This surface reaction was found to improve foam stability. In contrast to this situation it was reported that SiC looses its ability to stabilise a melt after overheating. XRD analysis showed the formation of Al_4C_3 in the melt at 950°C [52]. The microstructure of the bubble remnants produced under these conditions showed a wavy surface.

There is some evidence that the contact angle of the particles is the determining parameter in liquid-metal foam stability [47]. Therefore, selecting stabilising particles by exploiting tabulated data for contact angles [70] could be a successful strategy. In the example given in the previous paragraph, carbide formation on the surface of stabilising SiC particles probably modifies the contact angle of the particle putting it outside the preferred region.

Foamability of an Al composite containing TiB_2 particles (AlSi10+15wt.% TiB_2 particles of 3-6 µm size) was also examined [47]. The contact angle between TiB_2 and pure liquid Al is reported to be 98° at 900°C [113] although one has to be aware of differing data giving values down to 0° [114]. It was attempted to create aluminium foam by gas injection into the melt at 700°C and found that TiB_2 is not an effective stabiliser for this particular system. Only irregular bubble remnants could be produced. TiB_2 particles fall out from the bubble surfaces into the bubbles leaving a significant amount of powder of the surface of the melt. Particles can be extracted from a melt only if they are not wetted, indicating that TiB_2 is actually not wetted in this particular situation.

An additional important effect on foamability and microstructure is created by the reaction of the liquid metal with an oxidising blowing gas such as air [45,46]. In the presence of oxygen aluminium melts oxidise almost instantaneously. An oxide film continuously grows and reaches several hundred nanometres thickness. The oxidation effect on stability will be discussed in Sec. 5.2.2. At the moment we concentrate on its influence on surface segregation of particles.

A typical oxide skin on the inner surface of an air-blown foam is shown in **Figure 13**.

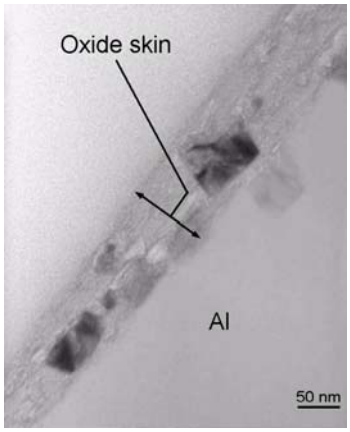

Figure 13. Oxide layer on the cell wall of a foam from a MMC (Cymat, Canada) [46].

Kommentar [JB5]: (TEMox)

Ip et al. suggested that complete coverage of the bubble surface by particles is not required to attain stable liquid-metal foam and assumed a minimum surface coverage of 50% [48]. The maximum surface coverage of Al_2O_3 and SiC particles in Metcomb foams was found to be 45% when nitrogen was used for foaming. The uniform coverage of a cell wall can be seen for Metcomb foams containing Al_2O_3 particles in **Figure 14a**. The particle concentration in the call walls is much higher than in the raw material, sometimes approaching 30 vol.% [22] and the surface areas are especially enriched having a local concentration of 2-4.5 times the bulk value.

The surface coverage decreases when oxidising foaming gas is used [46]. Wrinkled oxide layers cover the cell wall surfaces whenever foams are blown with air or oxygen (**Figure 14b**). Such layers are similar to those observed on the surface of aluminium castings. In order to make the particles visible a cell wall surface was gently polished until the surface oxide layer had disappeared (**Figure 14b**). The surface coverage observed here did not exceed 26 %. The local surface concentration was found to be only 1.5 times the particle concentration of the raw material in this case.

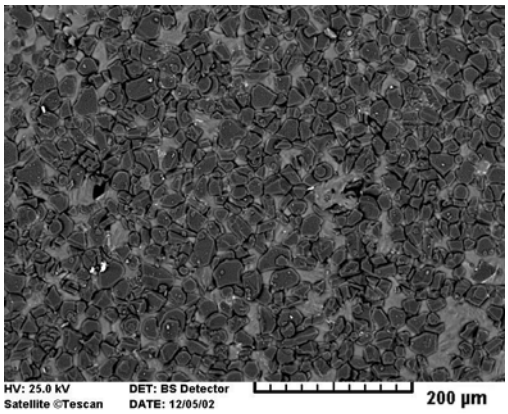

a) Untreated, foamed with *nitrogen*

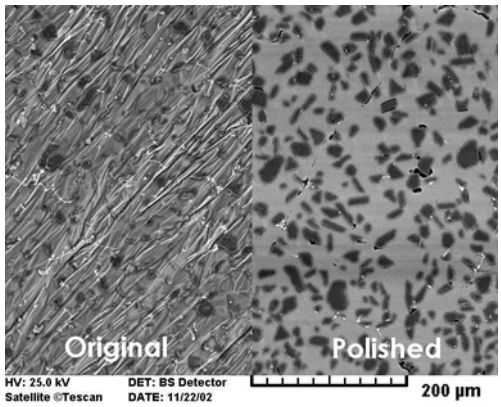

b) Left: untreated, right: polished with 1 µm sized SiC grains, foamed with *air*

Figure 14. Surfaces of a cell wall of Al_2O_3 particle containing Duralcan aluminium composite (W6D22A), SEM images [46].

Kommentar [JB6]: (surfcov_a b)

5.1.1.2 Added particles and internal gas blowing (Formgrip-type foams)

SEM analysis of cell walls in solidified Formgrip foams shows a dense coverage with particles if SiC particles with 13 µm average size are used (**Figure 15a**). If stabilisation with much larger particles (70 µm) is attempted the situation changes and only a small amount of the particles can be found on the surface (**Figure 15b**). The final cell wall thickness also varies with particle size: the 13 µm particles lead to cell walls about 85-100 µm thick, whereas the 70 µm particles increase the cell wall thickness up to 300 µm. Cross-sections of the cell walls of these two foams as shown in **Figure 15c** and **Figure 15d** confirm this picture.

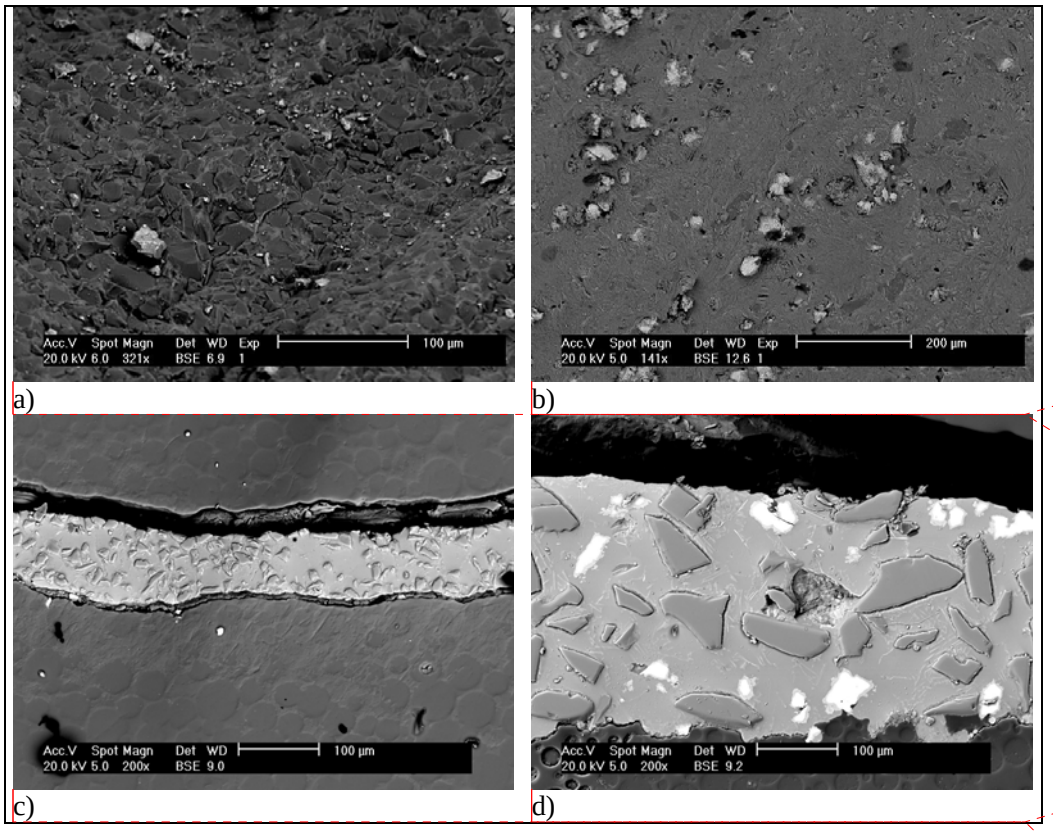

Figure 15. Upper row: Top view SEM image of a cell wall in a foam prepared from "Formgrip" material containing 10 vol.% SiC with a) 13 µm, b) 70 µm average diameter. Lower row: cross sections of same material: c) 13 µm, d) 70 µm particle [47].

Kommentar [JB7]: Formg13_cwsurf.

Kommentar [JB8]: Formg70_cwsurf.

Kommentar [JB9]: Formg13_cw.

Kommentar [JB10]: Formg70_cw

It is interesting that the high surface coverage with particles as shown by the face-on images (**Figure 15a** and **b**) is not so obvious in the cross-sections (**Figure 15c** and **d**). This might have created some doubts about the mechanism of particle stabilisation in the past. It is therefore always necessary to take images from both directions or to use 3D imaging techniques to obtain a reliable picture of the particle configuration.

5.1.1.3 Particles generated in-situ and external gas blowing

Particles can be generated in-situ by various means as listed in **Table 1**. One can rely on the solid component of a semi-solid melt or create oxides by in-situ oxidation. After injecting gas into such melts one could expect to obtain foams. Experimental

work shows that in reality it is hard to make foams in this way. It is interesting to show some results.

Pure aluminium melts were pre-treated for one hour bubbling air through it. This is known to lead to inner oxidation and to the formation of alumina particles. Following this treatment, it was possible to obtain bubbles at the surface which did not rupture immediately. However, the bubbles were not stable enough to form a stable foam layer. Coalescence and partial bubble collapse led to an onion-like structure into which bubble remnants piled up. The wall of one such bubble remnant showed a wavy surface [46]. It is interesting to compare this approach with patents from the 1960's [26] and 1970's [27,115] in which foam making processes were described based on pre-treating melts by inner oxidation and subsequently foaming them by addition of the gas-releasing blowing agent TiH_2. Reportedly, stable foams could be obtained in this way. We suspect that the alloy described in the patents led to an enhanced particle formation compared to the pure aluminium we used. Moreover, bubbles might be less prone to collapse when formed more gently by adding a gas-releasing blowing agent as compared to gas injection where the metal films are stretched rather quickly. Moreover, the strong movement of a large single bubble generated within the melt might lead to an agglomeration of oxide bifilms as observed for different materials by Körner et al. [50].

The Alporas foaming method leads to very homogeneous foams. The method uses a Al melt in which particles are created in-situ by adding Ca and allowing for oxidation. The question now is if it is possible to make stable foams from these melts by injecting gas instead of adding titanium hydride. A trial experiment on a AlCa3 alloy stirred for 30 min showed that bubbles of about 10 mm diameter are created in the melt which then rise to the top of the melt and merge there. However, some large bubble remains stable after some minutes of isothermal holding (see **Figure 2g**). A very inhomogeneous cell wall thickness distribution was found ranging from 10 µm until some hundred µm. The surface of the cells are wavy (**Figure 16a**). The foam microstructure contain many complex-shaped phases in the eutectic phase of the alloy (**Figure 16b**).

a). Wavy cell wall, optical micrograph (HMI)

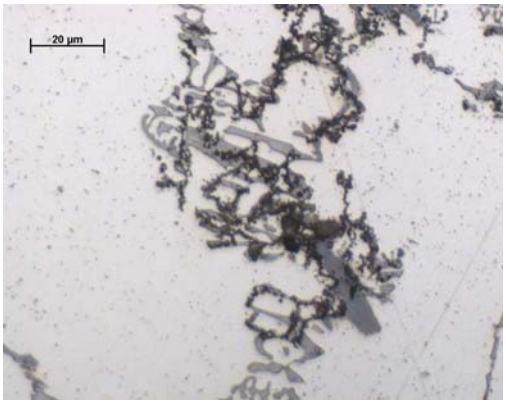

b). Complex shaped phase in the eutectic phase, cross section etched with 0.5% HF, optical micrograph (HMI).

Kommentar [JB11]: (Alpwave0107)

Kommentar [JB12]: (Alpfract0107)

Figure 16. "Foam" created by blowing a TiH_2-free Alporas precursor (same sample as shown in **Figure 2g**).

5.1.1.4 Particles generated in-situ and internal gas blowing (Alporas-type foams)

It is near at hand to ascribe the stabilisation effect in Alporas foams to the solid particles formed during stirring the aluminium alloy containing Ca under the influence of air which is dragged into the melt through the vortex [14]. Microstructural analysis of Alporas foams reveales the presence of oxides [46]. A commercial Alporas foam sample [116] was polished and etched with a 0.5 vol.% HF solution. SEM and EDX examinations show deeply etched valleys with high oxygen content and secondary phases attached to line-shaped pores with higher Ca and/or Ti content than the matrix. These line-shaped pores - most probably oxide bifilms [117] - form networks decorated with secondary phases. We suspect that these decorated bifilms play the crucial role in the stabilisation of Alporas-type metal foams. The size and volume fraction of these inclusions is estimated to be below 1 µm and 1 vol.%, respectively. No obvious segregation of these bifilms to the surface of the cell walls was found.

Recent investigation of the cell wall surface of the above mentioned Alporas foam sample show open bifilms (**Figure 17**). Another Alporas-type foam with different composition [118] clearly shows submicron-sized particles besides the bifilms (**Figure 18**). These particles could be primary crystals formed on the amorphous oxide skin during oxidation [119].

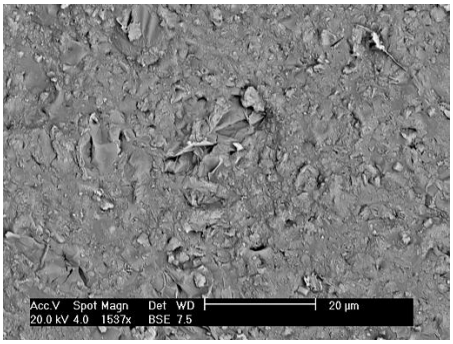

Figure 17. Open oxide bifilms on Alporas foams cell wall surface with surface concentration of 3.62 O, 4.51 Ca, 0.62 Ti, 3.62 Fe, rem. Al (in wt.%), SEM image (HMI).

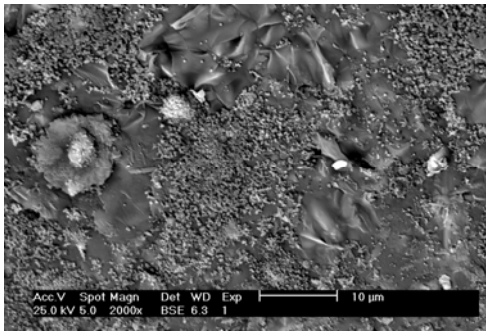

Figure 18. Surface of Alporas-type foam cell wall containing wrinkled oxide bifilms and submicron particles, with surface concentration of 9.06 O, 1.71 Ca, 0.35 Ti, rem. Al in wt %, SEM image (HMI).

Kommentar [JB13]: (Alpsurf jap)

Kommentar [JB14]: (Alpsurf)

Yang and Nakae [120] were able to produce foam from an AlSi7Mg0.5 alloy without any Ca addition. They stirred an alloy melt in air for 20 min with 600 rpm and added 5 wt.% Al powder with 60 µm particle diameter. After this foaming was triggered by TiH_2 addition. This technique actually combines oxide formation of the Alporas process with some ideas of the powder compact technique (see next paragraph). Because the aluminium powder added is oxidised, the oxide films entrained in the liquid assist foaming in addition to the oxides created during stirring.

5.1.1.5 Molten powder compacts and internal gas blowing (Alulight-type foams)

Foams are produced by melting powder compacts containing a blowing agent. It has been shown that the oxygen content of the precursor material is crucial for the stability of such foams. A study by Weigand showed that aluminium powders with

very low oxide contents did not lead to very stable foams [67] and a similar observation was made recently when argon and air atomised aluminium powders were compared [50]. Air atomised powders not only exhibit a higher oxide content but also a distribution of oxygen which includes the interior of each powder particle [50,67]. In lead foams [14,80] a similar dependence of foam stability on oxide content was found. Foams containing 0.06 wt.% oxygen did foam but drainage and foam collapse lead to strong and continuous drainage during the foaming stage. A content of 0.16 wt.%, however, lead to stable foams. **Figure 19** shows the oxide phases in a melted pure aluminium powder compact (not containing any blowing agent).

Wübben et al. used micro-gravity experiments to demonstrate that the primary action of the solid stabilising component of powder compact foams is to prevent films from coalescing while their influence on viscosity was seen as less important [34].

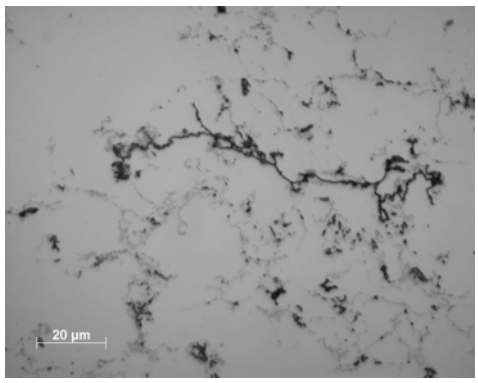

Figure 19. Complex phases in re-melted pure Al powder compact, optical micrograph (HMI).

Kommentar [JB15]: (0017P Metch01)

Foaming of pure Al powder compacts could be further stabilised with TiB_2, Al_2O_3, and SiC particle addition in this order [121].

5.1.1.6 Molten powder compacts and external gas blowing

Our recent trial to foam of Al-Si powder compact by foam generator was not successful (see **Figure 2f**). Although the same material can be foamed by internal gas creation (e.g. by embedded TiH_2 particles) this is not the case when the gas enters the liquid from one injection point.

5.1.2 Structure of cell walls

A quantitative characterisation of cell walls and Plateau borders is essential to understand the driving forces of stability. Cell wall thickness can be measured easily by analysing metallographic sections. More complex data such as curvature of Plateau borders requires 3D tomographic methods.

Many metal foams with low densities show a polyhedral cell structure with homogeneous cell wall thickness distributions between two Plateau borders [52]. Foams with higher densities usually have smaller and predominantly spherical cells mostly with diameters below 3 mm.

Although most metal foams show smooth cell walls (roughness in the range of the size of the solid particles present in the melt) some foams deviate from this pattern

especially when their cell walls contain agglomerated particles. This especially happens in foams made from powder compacts or in mixed particle systems (see **Figure 20**) [45,52].

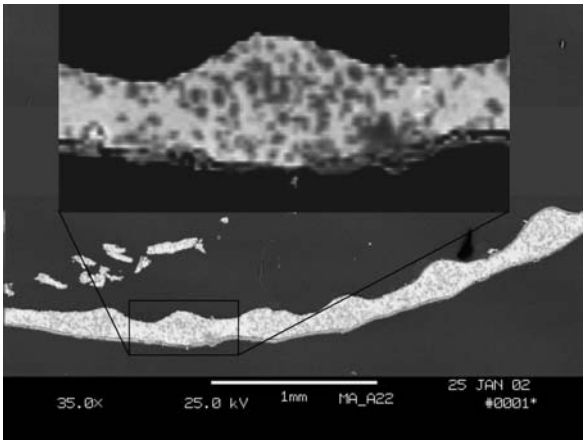

Figure 20. Wavy surface surrounding agglomerated particles `of cell wall made from AlMg1SiCu/**Al_2O_3/22**p raw material, SEM BS picture [52].

Kommentar [JB16]: (Aggl_in _cw)

Films of metallic melt cannot be stretched to such an extent as aqueous films. Liquid metallic films containing particles usually rupture below a critical thickness which ranges from about 30 to 150 µm [31] for foams made from powder compacts and slightly lower values for foams produced from metal matrix composites [45]. In the latter case it could be shown that the cell wall thickness depends on: a) the particle diameter – larger particles produce thicker, smaller particle thinner cells walls –, and b) the composition of the alloy, c) the particle composition of the material, and d) the foaming temperature [45,64].

The thickness data can be related to the disjoining forces acting between the interfaces in the cell wall. Detailed analysis of cell wall thickness of added particle foams has been carried out [45,46,52]. It was found that the surface composition of the particles is strongly related with the cell wall thickness. Alumina particles with spinel-coated surfaces lead to thicker cell walls than uncoated SiC particles of the same diameter [52]. Lognormal distributions of the cell wall thickness were found in all cases. In Metcomb foams no significant difference has been found between cell wall thicknesses of air and nitrogen-blown aluminium foams. The cell wall thickness also can depends on the collection efficiency of the particles by the bubble interface during foam evolution. Cell wall thickness increases with the travelling distance of bubbles, eventually reaching a saturation value [122].

Relationships between cell diameter and cell wall thickness of foams manufactured by Cymat (Canada) were given by Wood [123]. The cell wall thickness can be considered constant – around 50 µm – for large cell sizes above 8 mm diameter. At a diameter of 3 mm thickness is 85 µm.

Average and minimum cell wall thicknesses should be determined more systematically in the future, preferably as a function of particle parameters (size, shape, amount, bulk and surface composition, surface roughness), foams cell size, alloy characteristics (composition, temperature) and bubble pressure. The data already available at present is given in **Table 8**.

Table 8. Cell wall thickness of aluminium foams, all foam produced at 1 bar atmospheric pressure.

alloy	particle type and size [μm]	Minimum cell wall thickness, [μm]	Average cell wall thickness [μm]	Remark	Source
Foams blown by internal gas formation					
Al	Powder oxides	100	345		[124]*
Al99.9	Powder oxides		215	TiH_2 size 5 μm	[50]
Al99.9	Powder oxides		165	TiH_2 size 2 μm	[50]
AlSi2	Powder oxides	80	250		[124]*
AlSi6Cu4	Powder oxides	51		Measured in liquid	[31]*
AlSi7	Powder oxides	52		Measured in liquid	[31]*
AlSi7	Powder oxides	27-36	88		[125]
AlSi10Mg	Powder oxides	60-70	100-170		[126]*,**
AlSi10Mg0.6	Powder oxides	30-50		low resolution	[127]*,**
AlSi12	Powder oxides	80	205-320		[124]*
AlSi12Mg0.6	Powder oxides	60-80			[128]*,**
	In-situ oxides		~100		Own meas.
Al-9Si-0.5Mg	SiC (13)		~40		[24]*
Al-9Si-0.5Mg	SiC (63)		~210		[24]*
AlSi10Mg/	SiC (13)		~85		[47]*
AlSi10Mg	SiC (70)		~260		[47]*
Foams blown by external gas formation					
AlSi10Cu3Ni1.5	20% SiC (13)	20-30	55	0 min, 700°C, 10 mm	[52]
AlSi10Cu3Ni1.5	20% SiC (13)	33 (17 ox)	44	10 min, 700°C, 10 mm	[52]
AlSi10Cu3Ni1.5	20% SiC (13)	33	44	100 min, 700°C, 10 mm	[52]
AlSi10Mg	**12.5% Al_2O_3** (23)		35-50	no spinel, 0 min, 700°C, 10 mm	[52]
AlMg1SiCu	**10% Al_2O_3** (11)	30-43	112-86	spinel, 695-765°C, 10 min, 10 mm	[52]
AlSi10Cu3Ni1.5	**10% Al_2O_3** (11)	21	74	spinel, 725°C, 10 min, 10 mm	[52]
AlSi10Cu3Ni1.5Mg3	**10% Al_2O_3** (11)	20	61	spinel, 725°C, 10 min, 10 mm	[52]

* no temperature data, **estimated from a graphical representation

From the values of **Table 8** we can conclude that, 1) in foams blown by external gas formation the cell wall thickness does not decrease significantly with isothermal holding time (given in 5th column) [52]; 2) in both foaming routes addition of Mg and Si leads to a decrease of cell wall thickness; 3) the minimum cell wall thickness is 20-30 μm in aluminium foams; 4) spinel-coated Al_2O_3 particles yield thicker cell walls than SiC particles of the same size and volume fraction.

5.2 In-situ investigation of liquid metallic foams

In order to understand the evolution of metal foams it is useful to obtain data characterising the state of the foam *in-situ* during expansion while the metal foam is liquid. The technique which is probable the easiest to handle is the "expandometer" which is a specially constructed dilatometer for measuring foam volume as a function of time [129]. Other in-situ techniques which have been employed include thermoanalysis [130], thermogravimetry [131] and ultrasound probing [132]. All these techniques do not reveal the details of structural changes inside an evolving metal foam. In-situ X-ray monitoring experiments on metal foam yield such information. First experiments of that kind reportedly were carried out in the Alcan

laboratories 15 years ago [133]. With improved equipment such experiments were later carried out with synchrotron X-ray radiation [66], recently also using a laboratory X-ray source [134].

5.2.1 Foams created by internal gas evolution

Foamable precursors of different kinds were foamed and observed by in-situ X-ray radioscopy. Of the many results some connected to metal foam stability are reviewed here.

Foam evolution of both hot-pressed and thixo-cast foamable precursors of AlSi6Cu4 alloy containing TiH_2 as a blowing agent was investigated under normal atmosphere [135]. Applying an appropriate heating profile stable foams were found even after 10 minutes of isothermal holding in both the semisolid and liquid state (below and above liquidus temperatures, respectively). The difference between hot-pressed and thixo-cast precursors is shown in **Figure 21** which shows samples near maximum of expansion. Significant drainage was observed in the foam made from the thixo-cast sample while the foam made by foaming the pressed powder sample does not show any drainage. An explanation can be that the network of oxides is destroyed during thixo-casting, e.g. by agglomeration of the oxides to larger structures which are not effective in stabilisation. Such effects could be provoked by stirring molten powder compacts [50]. If this happens the delicate gel-like structure of interlocked filaments is damaged leading to increased drainage.

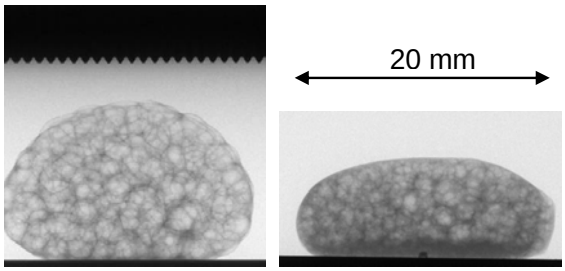

Figure 21. Radioscopic pictures of a hot pressed precursor foam (left) T = 600°C (below liquidus), thixocast precursor foam with strong drainage (right) T = 625°C (above liquidus) [136]. Width of samples is 20 mm.

Cell rupture is often observed when foamable precursors expand. Synchrotron radioscopy revealed that the time for liquid films to disappear lies below 55 ms [31].

Recent investigations on “Formgrip” foams by x-ray radioscopy show the effect of particle size on stability very clearly. Precursors containing two types of SiC particles were foamed under equal conditions and observed in-situ. It was found that bubble coalescence was much more pronounced for the precursor containing the coarse (i.e. 70 μm) particles than for the finer particles (i.e. 3 and 13 μm). **Figure 22** shows a late foaming stage of two foams. Obviously, the foam stabilised with fine particles is still stable while the one containing coarse particles has already collapsed.

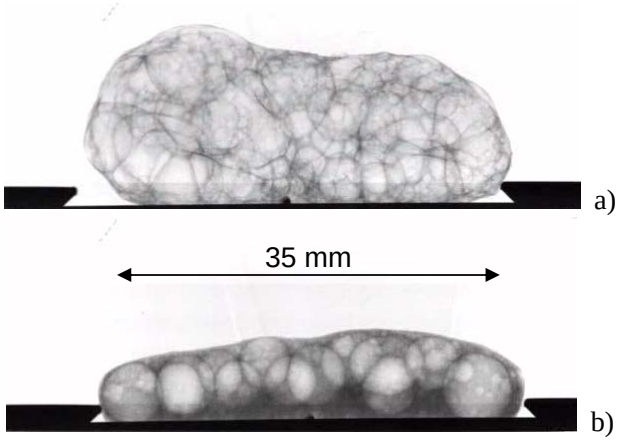

Figure 22. Liquid-Al foam stabilised particles produced from "Formgrip" precursors containing AlSi9Cu3 + 10 vol.% SiC and 0.5 wt.% TiH_2 as blowing agent, real-time X-ray radioscopy picture was obtained using a synchrotron beam [137]a) 13 μm SiC, b) 70 μm SiC.

5.2.2 Foams created by external gas injection

A recent investigation with high speed microfocus X-ray radioscopy showed during foaming of Metcomb-type foams with argon blowing the rupture time of the cells is below 40 ms (**Figure 23**).

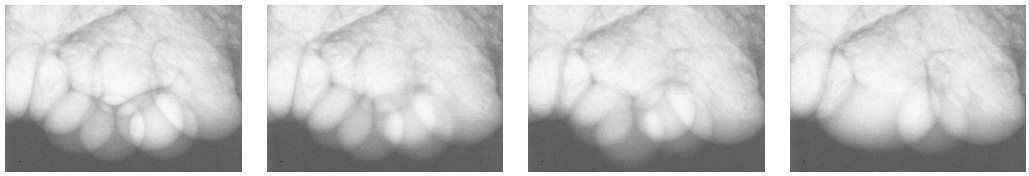

Figure 23. Rupturing of cell walls in Metcomb-type foam blown with argon. The exposition time of the individual images were set to 33 ms. 25 frames recorded per second. Width of each image is 14 mm. F3S20S Duralcan composite was used.

Drainage is a common and well investigated phenomenon in transparent aqueous foams. In order to characterise drainage in aluminium foams real-time X-ray radioscopic experiments were carried out on liquid-aluminium foam stabilised with SiC particles and blown with argon and air gases. The exposition time of each image was 110 ms. Particle stabilised aluminium foams were produced from F3S20S Duralcan metal matrix composite (MMC) precursor at 700°C. The foams were generated using Metcomb technology [22]. Bubbles of approximately 7 mm diameter in size were created on the bottom of the melt controlling the flow rate and the gas pressure with the foam generator of HKB, Austria. Approximately 42 and 25 cm^3 foams were produced applying 4.2 (argon) and 2.5 s (air) gas pulses, respectively [138].

The liquid-metal foam instantaneously forms a polyhedral structure. In spite of the significant flow of bubbles during foam formation, no foam rupture was detected at this stage of the process in the air-blown foams. Characteristic images of foam evolution – made by X-ray scanner – are shown in **Figure 24** and **Figure 25**. The two figures differ by the blowing gas used, corresponding to argon and air, respectively.

A diagram showing accumulated rupture events in argon-blown foam is shown in **Figure 26**. Air blown foam could not be evaluated because of the lack of rupture events. A diagram showing the vertical density profile of the foam as a function of height (drainage diagram) for argon-blown foam is shown in **Figure 27**. In these figures Φ_l represents the liquid volume calculated from integrals over horizontal lines of image intensities.

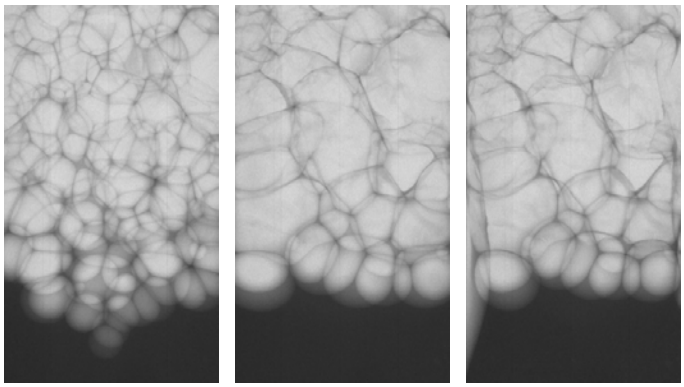

a) liquid b) liquid c) solid

Figure 24. Evolution of *argon*-blown foam shown by X-ray images. a) just after foam formation, b) at the end of isothermal holding (5 min), c) after solidification. Sample widths are 40 mm at the bottom [138].

Kommentar [JB17]: (Fig. 0049)

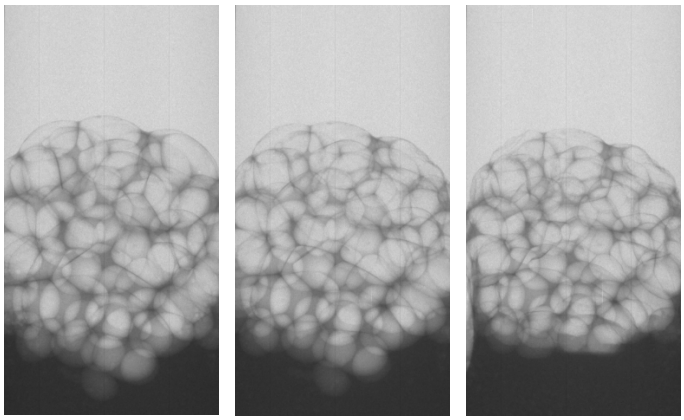

a) liquid b) liquid c) solid

Figure 25. Same as Figure 24 for *air*-blown foam [138].

Kommentar [JB18]: (Fig. 0050)

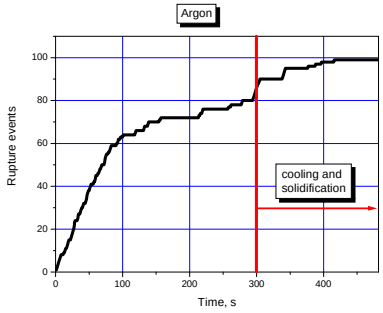

Figure 26. Accumulated rupture events in argon-blown foam [138].

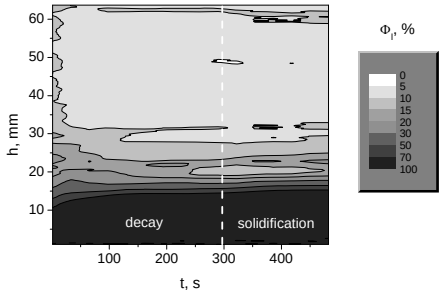

Figure 27. Drainage curves of *argon*-blown foam [138].

Kommentar [JB19]: (Fig. 0049rupture.)

Kommentar [JB20]: (Fig. 0049argonbw.)

The uniformity of bubble size is obvious from the first images in both **Figure 24** and **Figure 25** reflecting the situation just after foam creation. Isothermal holding leads to foam coarsening and a slight degradation of uniformity in argon-blown foams while air-blown foams remain almost unchanged. Air-blown foams are therefore stable against coalescence. It is known from previous ex-situ investigations [46] that a thick oxide skin develops on the inner surfaces of the cells whenever the foaming gas contains oxygen. This oxide skin improves largely the stability of foams. During solidification foams shrank significantly in both cases.

Argon-blown foams show some coalescence and drainage during isothermal holding. According to **Figure 26** coalescence is notable during the first 100 seconds and occurs at a roughly constant rate. It then levels off and is nearly constant for another 200 seconds. Cooling triggers some film rupture events which was already observed for Alulight-type foams before [31].

The drainage diagram in **Figure 27** shows significant drainage only in the first 20 seconds. In air-blown foam drainage was hardly detectable. This difference can be explained using experimental results on single Plateau borders of Koehler et al. [139] in aqueous foams. There it was shown that the mobility of film surfaces determines the drainage rate. Immobile surfaces slow down drainage. Using the analogy with aqueous foams the oxide can be considered as immobiliser of surfaces, thus leading to less drainage.

5.2.3 Synchrotron tomography

From the metallographic investigation of various metallic foams and an associated analysis of particle distributions in the cell walls the mechanism of stabilisation cannot be derived with certainty. Depending on the type of foam or the location of the images the picture varies. In some images the surface coverage of the metal films with particles is very clear (**Figure 11a**), while on other images portions of the surface devoid of particles can be detected (**Figure 15a**). It is not evident from the images how mechanical forces can be transmitted from on side of a film to the other via particle networks as postulated e.g. by Kaptay which would be required to create a disjoining force.

There are two explanations for these difficulties. Firstly, the two-dimensional character of metallographic analysis could obscure the structure of the postulated three-dimensional networks. Secondly, it is not guaranteed that the arrangement of particles in solid foams is identical to that in liquid foams. During cooling the

interaction of the solidification front with the particles – either engulfing or rejecting them – could change their arrangement to such an extent that the postulated networks cannot be detected in solid foams.

One way to obtain three-dimensional information is synchrotron tomography. Solid metal foams of the Formgrip-type (see Sec. 2.1) based on a AlSi10Mg matrix and stabilised with SiC particles of different sizes were investigated by high-resolution tomography with monochromatic radiation allowing for a separation of the two components [140]. The images obtained showed that the individual particles are indeed not all connected with each other and do not form networks which would allow for a transmission of forces across the cell walls. Therefore, the evidence from the metallographic studies does not seem to be an artefact of two dimensional imaging.

In order to assess possible effects during solidification in-situ tomography was carried out on liquid metal foams of the same composition [141]. The foams were created in a small glass cylinder which gave them some mechanical support after the end of the foaming process and prevented the foams from moving during the 20 minutes of exposure. Two tomograms were obtained in the liquid state after which the foams were solidified. Then one more tomogramme was taken. The data obtained was analysed by three-dimensional image analysis yielding the correlation between pores and SiC particles as shown in **Figure 28**. The left graph shows data corresponding to foams containing very coarse SiC powder which does not lead to stable foam. Quite clearly in the unfoamed state (which contains only few small pores) the correlation between bubbles and particles is weak. In the liquid state a pronounced correlation exists which becomes stronger with time. Solidification, however, does not change the picture very much. In foams stabilised with smaller SiC particles the picture looks different: from the unfoamed to the liquid foamed state the correlation increases to some extent. Solidification, however, leads to a big increase in correlation. Apparently the particle arrangement is changed by the advancing solidification front and particles are pushed to the surface. This could be an indication that networks of solid particles might exist in the liquid but cannot be detected after solidification. However, a direct proof for this is still lacking.

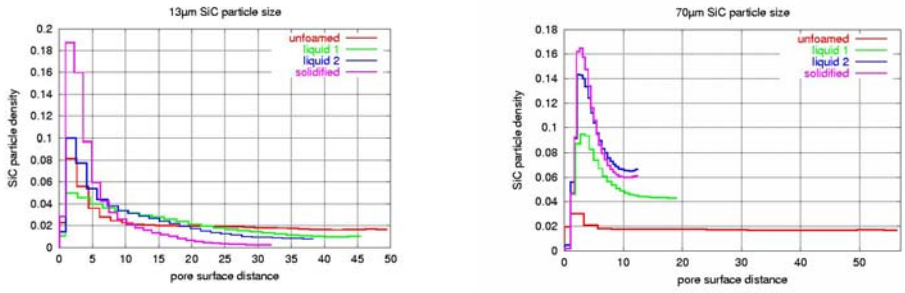

Figure 28. Correlation between individual SiC particles and pores in liquid Al foam as obtained by synchrotron tomography [141]. Foams containing a) 70 µm SiC particles, b) 13 µm SiC particles. Foam was created by melting same Formgrip precursor used for investigations discussed in Sec. 5.1.1.2 and 5.2.1.

6 Conclusions

The experimental work found in the literature demonstrates that probably all metal foams contain at least one solid phase which is responsible for stabilisation. The liquid in metal foams therefore forms a high temperature suspension or colloid. The origin, nature and spatial arrangement of the solid component in the fluid vary in different metal foam types. The way solid particles stabilise foams is only partially understood. Coming from aqueous or glass foams explanations in terms of viscosity, surface tension/elasticity and surface activity have been given. It is tempting to look for a unifying scheme according to which particles act and there have been claims that such a universal mechanism exists [50]. The present authors are sceptical that this is true and suspect that various distinct mechanisms apply.

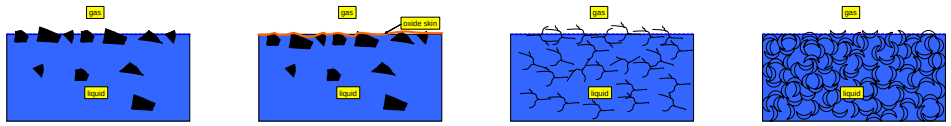

a) b) c) d)

Figure 29. Some of the particle-liquid configurations found in real metal foams (one liquid/gas interface shown): a) partially segregated particles on Metcomb-type foams blown with argon, b) the same system blown with oxidising blowing gas, c) partially connected bifilms in Alporas-type foam, d) interlocked oxide filaments in Alulight-type foams.

Foams of the *Metcomb- or Formgrip-type* are stabilised by individual, fairly large particles which can move around in the liquid. In solidified foams they seem to segregate preferentially at the liquid/gas interfaces of films with only a minor fraction of particles being in the interior of the films (**Figure 29a**). It is near at hand to give an interpretation in terms of models such as the LP2+C model by Kaptay (see **Figure 7c**). Accordingly, the particles are pinned to each of the interfaces of a film by means of interfacial forces. This would explain micrographs such as **Figure 11a** However it is not clear how the attractive interactions between the two interfaces are balanced. Kaptay postulates that mechanical forces are responsible for this counter-pressure – the disjoining pressure – which in his model are transferred through at least locally densely packed layers of particles. Experimental evidence, however, does not support the existence of such bridges between the two surface layers. The particles which are completely immersed in the liquid phase are not interconnected as shown clearly by high-resolution tomography [140]. However, there is some evidence that surface segregation of particles increases during solidification (**Figure 28**) so that the particle content in the liquid film could be higher in the liquid state than actually observed in the solid. This could be a loophole for saving the model since the existence of bridges connecting the two surface particle layers cannot be completely excluded. Another experimental fact is that there is no meniscus around individual particles sitting at each interface (see **Figure 12**) as one would expect from the picture of partially wetted particles. Instead, the interface is rather straight around particles. Furthermore, the oxide skin created during foaming with air plays an important role in stabilisation (**Figure 29b**). Such skins are not included in the current models of foam stability. In conclusion, we believe that the stabilisation mechanism of Metcomb- or Formgrip-type foams is still waiting for a full explanation.

Foams of the *Alulight-type* show a completely different stabilisation pattern. The existence of oxide filaments within aluminium powder particles, within pressed powder mixtures and within foams has been shown by various authors either by direct observation [50,67142] or indirectly by proving that low-oxide systems have a lower foam stability [50,80]. Wübben could even show that the oxide content is proportional to the inner surface area of foams [80]. These filaments do not segregate at the surface but rather span the entire volume of a film or Plateau border. The system of filaments is thought to hold the liquid aluminium alloy by capillary action or by merely locally enclosing small volumes of melt and preventing them to flow into the Plateau borders. The individual filaments seem to be interlocked so that they could act like a rigid sponge holding the liquid (**Figure 29d**). The system is quite fragile and seems to resemble a gel in terms of rheology. Poking into an aluminium foam with a steel needle can result in an outflow of melt. Körner et al. claim that individual oxide filaments form larger networks which form a kind of meta-particles with a huge internal porosity. They assume that these metaparticles stabilise the cell walls by forming an LP1-layer in Kaptay's notion (see **Figure 7**a) [50]. The idea sounds convincing but is based on very few and mostly indirect observations (e.g. the observed waviness of the cell walls). The traditional explanation that the foam is stabilised by the largely increased apparent viscosity of the liquid films by simply preventing fluid flow seems also possible at the current state of knowledge. To some extent the two viewpoints might not differ too much and the distinction between dynamic (viscosity-based) and static (surface-activity) based action might be more semantic in these gel-like fluids.

In addition to these foams *Alporas-type* foams exist in which oxide bi-films are created in-situ by reaction of the Al alloy with Ca or Mg under the presence of air. These films could act in a similar way to the oxide filaments in Alulight-type foams. Possibly the oxide filaments are less connected so that these foams are more fluid and can reach lower relative densities after full expansion (see **Figure 29c**).

Another point worth discussing is the possibility that a solid phase formed from the liquid during cooling into the semi-solid range of the phase diagram could stabilise foams. It was suspected that primary aluminium grains in foaming aluminium-silicon melts could enhance stability in addition to the oxide filament stabilisation mechanism [66]. As foams were observed to be also stable – although less – in the fully melted state this mechanism could not be responsible for stability alone and the literature is not specific on a mechanism of stabilisation (viscosity enhancement or surface activity). Körner later baptised this effect *endogeneous stabilisation* and made it responsible for the stability of Mg foams created in DCP foams [29]. She further suggests that the primary Mg particles are surface active and form layers analogous to the ceramic particles used for Metcomb-type foams. Although this idea is convincing there is no proof for it at present. Foams made by die-casting processing were obtained by injecting MgH_2 into pure Mg or Al [29,30]. As such processing can hardly be carried out in an oxygen-free environment spontaneous oxidation of the melt might also have added some oxides which then could have stabilised the foam. It remains to prove that alloys in the semi-solid state can be foamed in the absence of any reactive gas.

Finally, the foams made from extremely viscous metallic glasses present a challenge. Some of these foams show polyhedral cells which obviously are stabilised by interfacial forces, probably by remnants of the blowing agent B_2O_3 used [18]. Others, especially the foams in the early stages which are rather bubble dispersions, show

bubbles which have merged to one volume while still maintaining their original shape indicating the absence of interfacial stabilisation (see **Figure 2h**). This indicates the absence of stabilisation and the dominance of viscosity in foam formation.

In conclusion there are many open questions associated with metallic foams. More experimental work is required to clarify the role of solid particles in liquid metal colloid systems. Naturally, the main effort will be directed towards improving materials. The aim are aluminium foams with better stability, more uniform cell structures and cheaper manufacture. Improved liquid metal colloids could be open the road to such foams.

7 The Authors


Norbert Babcsán has been a postdoc in the metal foam group at the Technical University of Berlin and Hahn-Meitner-Institute in Berlin since 2003. He obtained his diploma in 1996 on the field of Engineering Physics with work related to single crystal growth. He spent one year at NASA Marshall Spaceflight Centre. Between 1996-2001 he was an assistant lecturer at the Department of Non-metallic Materials at University of Miskolc, Hungary. He acted as an organiser of three Junior Euromat Conferences and was scientific advisor for Leichtmetall-Kompetenzzentrum Ranshofen, Austria, where he carried out aluminium foam research between 2001-2002. He is one of the founders of ADMATIS Ltd., a Hungarian Space R&D company. He received his PhD at the University of Miskolc in 2003 on the field of Materials Science and Technologies. He is a winner of the Pro Sciencia and Science Award of the Hungarian Academy of Sciences. Email: babcsan@hmi.de

John Banhart is a professor in the Faculty of Material Science and Technology at the Technical University of Berlin and head of the Department of Materials Science at Hahn-Meitner-Institute in Berlin. Current working fields and research interests are light-weight materials including aluminium alloys, bulk metallic glasses, nanocrystalline alloy composites and metal foams. His department runs facilities for small-angle X-ray and neutron scattering and operates various methods for tomography. He is a physicist and earned his PhD in physical chemistry at the University of Munich in 1989. After working in theoretical alloy physics he changed to application oriented work at the Fraunhofer-Institute in Bremen where a process for foaming metals was developed in close cooperation with industry. He obtained his second degree (habilitation) in 1998 in Solid State Physics at the University of Bremen. Email: banhart@hmi.de

Acknowlegdements

Various people have supported us by providing samples of their foams or raw materials for foam making which we could use for further analysis: Vlado Gergely of Cambridge University, Bo-Young Hur of Chinju Korea, Dietmar Leitlmeier of LKR, Austria and Tetsuo Miyoshi, Japan. Astrid Haibel and Francisco García-Moreno have provided some graphs from their papers. Support by the European Space Agency (ESA) via an International Trainee Grant for one of us (N.B.) is gratefully acknowledged.

8 References

1 L. Gibson and M.F. Ashby, *Cellular Solids*, Cambridge University Press (1997)
2 B. Sosnick, US Patent 2 434 775 (1948)
3 J. C. Elliot, US Patent 2 751 289 (1956)
4 J. Banhart and D. Weaire, *On the road again: metal foams find favor*, Physics Today 55, 37-42 (2002)
5 S. Akiyama, K. Imagawa, A. Kitahara, S. Nagata, K. Morimoto, T. Nishikawa, M. Itoh, European Patent Application 0 210 803 A1 (1986)
6 W.W. Ruch and B. Kirkevag, WO Patent 9 101 387 (1991)
7 I. Jin, L.D. Kenny and H. Sang, US Patent 5 112 697 (1992)
8 B.C. Allen, M.W. Mote, A.M. Sabroff, US Patent 3 087 807 (1963)
9 J. Baumeister, *Verfahren zur Herstellung poröser Metallkörper*, German Patent 4 018 360 (1991)
10 J. Banhart, *Manufacture, characterisation and application of cellular metals and metallic foams*, Progress in Materials Science 46, 559-632 (2001)
11 H.P. Degischer and B. Kriszt, *Handbbook of Cellular Metals*, Wiley-VCH (2002)
12 http://www.metalfoam.net
13 J. Banhart, *Aluminium foams for lighter vehicles*, International Journal of Vehicle Design, in press (2005)
14 J. Banhart, *Manufacturing routes for metal foams*, Journal of Metals 52, 22-27 (2000)
15 F. Baumgärtner, I. Duarte, J. Banhart, *Industrialisation of P/M foaming process*, Adv. Eng. Mater. **2**, 168-174 (2000)
16 J. Pötschke, T. Hoster, P. Pant, Report to German Ministery of Science and Technology (BMFT), (1984)
17 M. Niemeyer, H. Haferkamp, D. Bormann, Mat.-wiss. u. Werkstofftech. 31, 419 (2000)
18 J. Schroers, C. Veazey, M.D. Demetriou and W.L. Johnson, Journal of Applied Physics, 96 (2004) 7723-7730
19 V. Shapovalov and L. Boyko, Adv. Eng. Mat., 6 (2004) 407
20 S.K. Hyun, H. Nakajima, Advanced Engineering Materials 4 (2002) 741-744
21 M.W. Kearns, P.A. Blenkinshop, A.C. Barber, T.W. Farthing, Int. J. Powder Met (1988); 24:59
22 D. Leitlmeier, H.P. Degischer and H.J. Flankl, Advanced Engineering Materials 4 (2002) 735-740
23 http://www.alulight.com
24 V. Gergely, T.W. Clyne, Advanced Engineering Materials, 2 (2000) 175
25 J. Banhart, J. Baumeister, A. Melzer, M. Weber, *Verfahren zur Herstellung von Verbundwerkstoffbauteilen*, German Patent DE 198 13 176 (1998)
26 W. S. Fiedler, US Patent 3 214 265 (1965)
27 C. B. Berry Jr., US Patent 3 669 654 (1972)
28 K. Renger, H. Kaufmann, *Vacuum foaming of magnesium slurries*, preprint (2005)
29 C. Körner, M. Hirschmann, V. Bräutigam and R.F. Singer, Advanced Engineering Materials 6 (2004) 385-390
30 W. Knott, B. Biedermann, M. Recksik, A. Weier, German Patent Application DE 101 27 716 (2001)

31 H. Stanzick, M. Wichmann, J. Weise, J. Banhart, L. Helfen, T. Baumbach, *Process control in aluminium foam production using real-time x-ray radioscopy*, Adv. Eng. Mater. **4**, 814-823 (2000)

32 B. Matijasevic, S. Fiechter, I. Zizak, O. Görke, N. Wanderka, P. Schubert-Bischoff, J. Banhart, *Decomposition behaviour of as-received and oxidised TiH2 powder*, in: Proc. PM2004 World Congress, Ed.: H. Danninger, R. Ratzi, EPMA, Vol. 4, pp. 149-155

33 European Space Agency, Erasmus Experiment Archive, http://spaceflight.esa.int/eea

34 T. Wübben, H. Stanzick, J. Banhart and S. Odenbach, *Stability of metallic foams studied under microgravity*, J. Phys.: Condens. Matter 15 (2003) 427-433

35 J. Banhart, *Development of advanced foams under microgravity*, in: D. Weaire and J. Banhart [Eds.], Foams and Films, MIT-Verlag Bremen (1999) p. 73

36 D. Weaire and S. Hutzler, *The Physics of Foams*, (Oxford University Press, Oxford 1999)

37 J.J. Bikerman, Foams, (Springer-Verlag New York Inc., 1973)

38 D. Exerowa and P.M. Kruglyakov, *Foam and foam films*, (Elsevier, 1998)

39 P. R. Garrett, *Defoaming: theory and industrial application*, (Marcel Dekker Inc., New York 1993)

40 A.J. Wilson, *Foams: Physics, Chemistry and Structure*, (Springer Series in Applied Biology, Vol 1, 1989)

41 E. Dickinson and G. Stainsby, *Advances in Food Emulsions and Foams*, (Elsevier Applied Science, 1988)

42 K. L. Mittal and P. Kumar, *Emulsions, Foams, and Thin Films*, (Marcel Dekker, 2000)

43 I. D. Morrison and S. Ross, *Colloidal Dispersions: Suspensions, Emulsions, and Foams*, (Springer, 1989)

44 L.L. Schramm, *Emulsions, Foams, & Suspensions - Fundamentals & Applications*, (VCH Verlagsgesellschaft mbH, 2005)

45 N. Babcsán, D. Leitlmeier and H. P. Degischer, Materialwissenschaft und Werkstofftechnik 34 (2003) 22-29

46 N. Babcsán, D. Leitlmeier, H.-P. Degischer, J. Banhart, *The role of oxidation in blowing particle-stabilised aluminium foams,* Adv. Eng. Mat. 6 (2004), 421-428

47 N. Babcsán, D. Leitlmeier and J. Banhart, *Metal Foams – High Temperature Colloids*, Colloids and Surfaces A, (2005) in press

48 S.W. Ip, Y. Wang and J.M. Toguri, *Aluminium foam stabilization by solid particles*, Can. Met. Quart., 38 (1999) 81.

49 V. Gergely and T.W. Clyne, Acta Materiala 52 (2004) 3047-3058

50 C. Körner, M. Arnold and R.F. Singer, Mat. Sci. and Eng. A, in press

51 D. Kenny, private communication

52 N. Babcsán, Ph.D. dissertation, University of Miskolc, 2003.

53 A.I. Rusanov and V.V. Krotov, *Gibbs elasticity of liquid films, threads and foams*, Prog. Surf. Membrane Sci. 13 (1979) 415-524

54 A. Prins and M. van den Tempel, J. Phys. Chem., 73 (1969) 2828

55 P. M. Claesson and M.W. Rutland, in Krister Holmberg (Eds.), *Handbook of Applied Surface and Colloid Chemistry*, John Wiley and Sons Ltd., 2001, p. 933.

56 P.M. Claesson and M.W. Rutland. *Measuring Interaction between Surfaces*, in Handbook of Applied Surface and Colloid Chemistry, ed. K. Holmberg, (John Wiley& Sons, Ltd., 2001) pp. 934-964

57 B.P. Binks, Current Opinion in Colloid and Interface Science, 7 (2002) 21.
58 A.D. Nikolov and D.T. Wasan, Langmuir, 8 (1992) 2985.
59 J.C. Wilson, *A study of particulate foams*. Ph.D. thesis, University of Bristol (UK), 1980.
60 G. Johansson and R.J. Pugh, International Journal of Mineral Processing, 34 (1992) 1.
61 Y.Q. Sun and T.Gao, Metall. Trans., 33A (2002) 3285.
62 T. Okubo, Journal of Colloid and Interface Science, 171 (1995) 55.
63 C. Nexhip, S. Sun and Jahanshahi, *Some observation on the drainage of CaO-SiO2-Al2O3 slag bubble films*, Metall. Mater. Trans. B., 31B (2000) 1105-1115
64 V. Gergely, L. Jones and T.W. Clyne, Trans. JWRI, 30 (2001) 371.
65 H. Kumagai, Y. Torikata, H. Yoshimura, M. Kato and Yano, Agric. Biol. Chem., 55 (1991) 1823-1829
66 J. Banhart, H. Stanzick, L. Helfen and T. Baumbach, *Metal foam evolution studied by synchrotron radioscopy*, Applied Physics Letters, 78 (2001) 1152-1154
67 P. Weigand, *Untersuchung der Einflußfaktoren auf die pulvermetallurgische Herstellung von Aluminiumschäumen*, Bremen, Germany: MIT-Verlag, (1999)
68 C. Körner, M. Thies and R.F. Singer, Advanced Engineering Materials, 4 (2002) 765-769
69 G. Kaptay, in J. Banhart, M.F. Ashby, N.A. Fleck (Eds.), Cellular Metals and Metal Foaming Technology, MIT-Verlag, Bremen, 2001, p. 117.
70 G. Kaptay, Colloids and Surfaces A, 230 (2004) 67.
71 G. Kaptay, *On surface properties of molten aluminum alloys of oxidised surface*, Materials Science Forum Vol. 77 (1991) pp. 315-330
72 A. Pamies, C. Garcia Cordovilla and E. Louis, *The measurement of surface tension of liquid aluminum by means of the maximum bubble pressure method: the effect of surface oxidation*, Scripta Metallurgica, 18 (1984) 869-872
73 R.A. Saravanan, J.M. Molina, J. Narciso, C. Garcia-Cordovilla and E. Louis, *Effect of nitrogen on the surface tension of pure aluminum at high temperature*, Scripta mater. 44 (2001) 965-970
74 R.A. Saravanan, J.M. Molina, J. Narciso, C. Garcia-Cordovilla and E. Louis, *Surface tension of pure aluminum in argon/hydrogen and nitrogen/hydrogen atmospheres at high temperature*, Journal of Materials Science Letters, 21 (2002) 309-311
75 G. Kaptay, E. Bader, L. Bolyan, *Interfacial Forces and Energies Relevant to Production of Metal Matrix Composites*, Materials Science Forum, 329-330 (2000) 151-156
76 C.Garcia-Cordovilla, E. Louis, A. Pamies, *The surface tension of liquid pure Al and Al-Mg alloys*, Journal of Materials Science, 21 (1986) 2787-2792
77 E. Ricci, A. Passerone, P. Castello, P. Costa, J. Mater. Sci., 29 (1994) 1833-1846
78 E. A. Howell, C.M. Megaridis, M. McNallan, Int. J. of Heat and Fuid Flow, 25 (2004) 91-102
79 D. Brabazon, D.J. Brown and A.J. Carr, Mat. Sci. and Eng. A356 (2003) 69-80
80 T. Wübben, PhD Thesis, University of Bremen (2003)
81 L. Ma and Z. Song, Scripta Materiala, 39 (1998) 1523-1528
82 T. Iida and R.I.L. Guthrie, *The Physical Properties of Liquid Metals*, (Clarendon Press, Oxford, 1988)

83 D. Klempner and K.C. Frisch, *Handbook of polymeric foams and foam technology*, Hanser Publishers, (1991)
84 S.M. Jung and R.J. Fruehan, ISIJ International, 40 (2000) 348-355
85 D.S. Viswanath and G. Natarajan, *Data book on the viscosity of liquids*, (Imprint New York : Hemisphere Pub. Corp., 1989)
86 H.K. Moon, J.K. Cornie and M.C. Flemings, Mat. Sci. and Eng., A144 (1991) 253-265
87 H.P. Degischer, *Recycling of Metal Matrix Composites*, Encyclopedia of Materials: Science and Technology, Elsevier Science Ltd. (2001) 5452-5455
88 J. Fjellstedt, A.E.W. Jarfors and L. Svendsen, *Experimental analysis of the intermediary phases AlB2, AlB12 and TiB2 in the Al–B and Al–Ti–B systems*, Journal of Alloys and Compounds 283 (1999) 192–197
89 K.B. Lee, J.P. Ahn and H. Kwon, *Characteristics of AA6061/BN Composite Fabricated by Pressureless Infiltration Technique*, Metall. Trans. A, 32A (2001) 1007-1018
90 K.B. Lee and H. Kwon, *Fabrication and Characteristics of AA6061/Si3N4 Composite by the Pressureless Infiltration Technique*, Metall. Trans. A, 30A (1999) 2999-3007
91 S. Akiyama, H. Ueno, K. Imagawa, A. Kitahara, K. Morimoto, T. Nishikawa and M. Itoh, US Patent 4 713 277 (1987)
92 V. Gergely, H.P. Degischer and T.W. Clyne, *Recycling of MMCs and production of metallic foams*, in Comprehensive Composite Materials, 3 (2000) 797-820
93 M. Thomas, D. Kenny and H. Sang, US Patent 5 622 542 (1997)
94 E.Y. Gutmanas and I. Gotman, *Dense High-temperature Ceramics by Thermal Explosion Under Pressure*, Journal of the European Ceramic Society 19 (1999) 2381-2393
95 T.P.D. Rajan, R.M. Pillai and B.C. Pai, *Reinforcement coatings and interfaces in aluminum metal matrix composites*, J. Mater. Sci., 33 (1998) 3491-3503
96 S. Vaucher and O. Beffort, *Bonding and interface formation in Metal Matrix Composites*, MMC-Assess Thematic Network, EMPA Thun, Switzerland, Vol. 9. (2001), http://mmc-assess.tuwien.ac.at
97 V.M. Bermudez, *Auger and electron energy-loss study of the Al/SiC interface*, Appl. Phys.Lett., 42 (1983) 70-72.
98 D.J. Lloyd, *The solidification and microstructure of particulate reinforced Al/SiC composites*, Compos. Sci. Tech., 35 (1989) 159-180
99 C. Cayron, EMPA report Nr 250, Thun, Switzerland (2001)
100 J.C. Viala, P. Foretier and J. Bouix, *Stable and metastable phase-equilibria in the chemical interaction between aluminum and silicon-carbide*, J. Mater. Sci., 25 (1990) 1842-1850
101 A. Bardal, *Wettability and interfacial reaction products in the AlSiMg surface-oxidised SiC system*, Mat. Sci. and Eng., A159 (1992) 119-125
102 ALCAN: World Patent WO9317139, (1993)
103 ALCAN: World Patent WO9308311, (1993)
104 D.M. Schuster, M.D. Skibo, *The recycling and reclamation of MMCs*, J. Met., 45 (1993) 26-30
105 M.S. Yaghmaee and G. Kaptay: *On the Stability Range of SiC in Ternary Liquid Al-Si-Mg Alloy*, Volume 2 - No 3 - July 2001, Electronic Proceeding of the

Hungarian Society of Materials World, http://www.materialworld.uni-miskolc.hu/
106 A.D. McLeod, and C.M. Gabryel, *Kinetics of the Growth of Spinel on Alumina Particulate in Aluminium Alloys Containing Magnesium*", Metall. Trans.,23A (1992) 1279-1283
107 T. Onda, S. Shibuichi, N. Satoh and K. Tsujii, Langmuir,12 (1996) 2125
108 D.S. Han, H. Jones and H.G. Atkinson, *The wettability of silicon-carbide by liquid aluminum - the effect of free silicon in the carbide and of magnesium, silicon and copper alloy additions to the aluminum*, J. Mater. Sci., 28 (1993) 2654-2658.
109 V. Laurent, D. Chatain, D. Chatillon and N. Eustatohopoulos, Acta Metall., 36 (1988) 1797-1803
110 V. Laurent, C. Rado and N. Eustathopoulos, *Wetting kinetics and bonding of Al and Al alloys on α-SiC*, Materials Science and Engineering, A205 (1996) 1-8
111 S. Suresh, A. Mortensen and A. Needlman, Fundamentals of Metal-Matrix Composites, Butterworth-Heinemann (1993)
112 P. Shen, H. Fujii, T. Matsumoto, K. Nogi, Wetting of (0001) α Al_2O_3 single crystals by molten Al, Scripta Materiala, (2003) to be published
113 A.R. Kennedy, in N. Eustathopoulos and N. Sobczak (Eds.) Proc. Int. Conf. High Temperature Capillarity, 29. June – 2. July 1997, Cracow, 1997 p. 395.
114 G.Kaptay, E.Báder, L.Bolyán, Materials Science Forum, 329-330 (2000) 151.
115 L.M. Niebylski, C.P. Jarema, T.E. Lee, US Patent 3 816 952 (1974)
116 supplied by Dr. Miyoshi from Japan
117 J. Campbell, Castings: *The New Metallurgy of Cast Metals*, Butterworth-Heinemann 2nd edition, 2003.
118 supplied by Prof. Bo Young Hur from Korea
119 G.M. Scamans and E.P. Butler, *In Situ Observation of Crystalline Oxide Formation During Aluminum and Aluminum Alloy Oxidation*, Metall. Trans. A., 6A (1975) 2055-2063
120 C.C. Yang and H. Nakae, Journal of Materials Processing Technology, 141 (2003) 202-206
121 A.R. Kennedy and Asavavisithchai, in J. Banhart, N.A. Fleck, A. Mortensen (Eds.), Cellular Metals and Metal Foaming Technology,MIT-Verlag, Berlin, 2003, p. 147.
122 N. Babcsán and D. Leitlmeier, unpublished work
123 J.T. Wood, *Production and Application of Continuously Cast, Foamed Aluminum*, in 'Metal Foams', eds. J. Banhart and H. Eifert, MIT-Verlag, Bremen (1998) 31-35
124 B. Kriszt, P. Cekan, K. Faure, *Foamability of the Al-Si system*, In: Cellular Metals and Metal Foaming Technology (Ed.: J. Banhart, M.F. Ashby, N.A. Fleck), Verlag MIT, Bremen (2001), 77-82
125 O. Brunke, S. Odenbach, and F. Beckmann, *Quantitative methods for the analysis of synchrotron- μCT datasets of metallic foams*. Euopean Physical Journal of Applied Physics 29, 73-81 (2005)
126 C. Körner, F. Berger, M. Arnold, C. Stadelmann, R.F. Singer, *Influence of processing conditions on morphology of metal foams produced from metal powder*, Mat. Sci. Tec. 16 (2000) 781

127 B. Olurin, M. Arnold, C. Körner, R.F. Singer, *The investigation of morphometric parameters of aluminium foams using micro-computed tomography*, Mat. Sci. Eng. A328 (2002) 334
128 A.E. Markaki, T.W. Clyne, *Characterisation of impact response of metallic foam / ceramic laminates*, Mat. Sci. Tec. 16 (2000) 785
129 J. Banhart, J. Baumeister, M. Weber, *Powder metallurgical technology for the production of metal foam.* Proceedings of the European Conference on Advanced PM Materials, Birmingham 23.-25.10.1995 (1995), p. 201-208
130 D. Lehmhus, G. Rausche, Adv. Eng. Mater
131 F. von Zeppelin, M. Hirscher, H. Stanzick, J. Banhart, *Desorption of hydrogen from blowing agents used for foaming metals*, Composite Science and Technology 63, 2293-2300 (2003).
132 U. Laun, J. Banhart, *Sound transmission study on liquid foams*, in: Cellular Metals and Metal Foaming Technology (Proc. MetFoam2001), Editors: J. Banhart, M.F. Ashby, N.A. Fleck, MIT-Verlag Bremen (2001), p. 255
133 I. Jin, private communication (2004)
134 F. Garcia-Moreno, M. Fromme, J. Banhart, in: *Real time X-ray radioscopy on metallic foams using a compact micro-focus source*, In: Cellular metals and metal foaming technology, Editors: J. Banhart, N.A. Fleck, A. Mortensen, pp. 89-94, MIT-Verlag, Berlin (2003)
135 F. García-Moreno, N. Babcsán and J. Banhart, *X-ray radioscopy of liquid metal foams: influence of heating profile, atmosphere and pressure*, Colloids and Surfaces A. (2005) in press
136 F. Garcia-Moreno, N. Babcsán, J. Banhart, M. Haesche, J. Weise, *Cellular Metalls and Polymers*, Editors: R.F. Singer, C. Körner, V. Altstädt, in press
137 N. Babcsán, J. Banhart, D. Leitlmeier, *Metal Foams – Manufacure and Physics of Foaming*, in: Advanced Metallic Materials, Eds: J. Jerz, P. Sebo, M. Zamánkovà, Bratislava (2004), pp. 5-15
138 N. Babcsán, F. García-Moreno, D. Leitlmeier, J. Banhart, *Liquid-metal foams – a perspective for feasible in-situ experiments under low gravity*, Materials Science Forum, (2005) accepted
139 S.A. Koehler, S. Hilgenfeldt, E.R. Weeks and H.A. Stone, Phys. Rev. E66 (2002) 040601(R)
140 A. Haibel, unpublished work
141 A. Haibel, A. Bütow, A. Rack, J. Banhart, *Quantitative analysis of pore-particle correlations in metallic foams.* 16th World Conference on Non-destructive Testing, Montreal, 30.08.-03.09.2004
142 M. Weber, PhD Thesis, MIT-Verlag Bremen (1995)